Commissioning and quality assurance for VMAT delivery systems: An efficient time-resolved system using real-time EPID imaging

Benjamin J. Zwan[1,2], Michael P. Barnes[3,4], Jonathan Hindmarsh[1], Seng B. Lim[5], Dale M. Lovelock[5], Todsaporn Fuangrod[3], Daryl J. O'Connor[2], Paul J. Keall[6], Peter B. Greer[2,3]

[1] Central Coast Cancer Centre, Gosford Hospital, Gosford, NSW, 2250, Australia
[2] School of Mathematical and Physical Sciences, University of Newcastle, Newcastle, NSW, 2308, Australia
[3] Department of Radiation Oncology, Calvary Mater Hospital, Newcastle, NSW, 2298, Australia
[4] School of Medical Radiation Sciences, University of Newcastle, Newcastle, NSW, 2308, Australia
[5] Department of Medical Physics, Memorial Sloan-Kettering Cancer Centre, New York, NY, 10065, U.S.A.
[6] Radiation Physics Laboratory, Sydney Medical School, University of Sydney, Sydney, NSW 2006, Australia

Corresponding author: Benjamin J. Zwan
Full mailing address: Central Coast Cancer Centre, Holden St, Gosford, NSW, 2250, Australia
Telephone: (02) 43 209 868
Email address: Benjamin.Zwan@health.nsw.gov.au

Conflicts of interest and financial disclosures: None

ABSTRACT

Purpose: An ideal commissioning and quality assurance (QA) program for Volumetric Modulated Arc Therapy (VMAT) delivery systems should assess the performance of each individual dynamic component as a function of gantry angle. Procedures within such a program should also be time-efficient, independent of the delivery system and be sensitive to all types of errors. The purpose of this work is to develop a system for automated time-resolved commissioning and QA of VMAT control systems which meets these criteria.

Methods: The procedures developed within this work rely solely on images obtained using an electronic portal imaging device (EPID) without the presence of a phantom. During the delivery of specially designed VMAT test plans, EPID frames were acquired at 9.5 Hz using a frame grabber. The set of test plans was developed to individually assess the performance of the dose delivery and multileaf collimator (MLC) control systems under varying levels of delivery complexities. An in-house software tool was developed to automatically extract features from the EPID images and evaluate the following characteristics as a function of gantry angle: dose delivery accuracy, dose rate constancy, beam profile constancy, gantry speed constancy, dynamic MLC positioning accuracy, MLC speed and acceleration constancy, and synchronisation between gantry angle, MLC positioning and dose rate. Machine log files were also acquired during each delivery and subsequently compared to information extracted from EPID image frames.

Results: The largest difference between measured and planned dose at any gantry angle was 0.8% which correlated with rapid changes in dose rate and gantry speed. For all other test plans the dose delivered was within 0.25% of the planned dose for all gantry angles. Profile constancy was not found to vary with gantry angle for tests where gantry speed and dose rate were constant, however, for tests with varying dose rate and gantry speed, segments with lower dose rate and higher gantry speed exhibited less profile stability. MLC positional accuracy was not observed to be dependent on the degree of interdigitation. MLC speed was measured for each individual leaf and slower leaf speeds were shown to be compensated for by lower dose rates. The test procedures were found to be sensitive

to 1 mm systematic MLC errors, 1 mm random MLC errors, 0.4 mm MLC gap errors and synchronisation errors between the MLC, dose rate and gantry angle controls systems of 1˚. In general, parameters measured by both EPID and log files agreed with the plan however a greater average departure from the plan was evidenced by the EPID measurements.

Conclusion: QA test plans and analysis methods have been developed to assess the performance of each dynamic component of VMAT deliveries individually and as a function of gantry angle. This methodology relies solely on time-resolved EPID imaging without the presence of a phantom and has been shown to be sensitive to a range of delivery errors. The procedures developed in this work are both comprehensive and time-efficient and can be used for streamlined commissioning and QA of VMAT delivery systems.

I. INTRODUCTION

Volumetric-modulated arc therapy (VMAT) is a modern radiotherapy delivery technique where an external beam of radiation is delivered during continuous gantry rotation. Highly conformal 3D dose distributions are delivered by dynamically shaping the radiation beam using a multi-leaf collimator (MLC) and through continuous modulation of the dose rate (DR) and gantry speed (GS).[1, 2] Compared to intensity-modulated radiation therapy (IMRT),[3] where the gantry is static during dose delivery, VMAT requires fewer monitor units (MU) and generally shorter treatment times to achieve an equivalent dose distribution.[2, 4] A potential disadvantage for VMAT is the added complexity related to more intricate dynamic MLC trajectories, DR modulation and changes in GS.

Due to this high level of complexity there is a need for more comprehensive linear accelerator (linac) commissioning and quality assurance (QA) techniques to properly assess the performance of the individual VMAT control systems. One challenge for VMAT commissioning and QA systems is the ability to assess the synchronisation of each of the 3 dynamic components (i.e. the MLC, DR and GS). It is also essential that commissioning and QA programs are independent of the linac control system, time-efficient enough to perform on a regular basis and have the ability not only to detect errors but also to determine their source.

Commissioning and QA procedures specific to VMAT delivery systems have been proposed using integrated images from an electronic portal imaging device (EPID).[5-10] The most commonly applied procedures for the Varian RapidArc platform (Varian Medical Systems, Palo Alto, CA) were developed by Ling et al.[5] who proposed tests designed to evaluate the performance of the linac delivery system in a step-wise manner. Tests were designed to assess MLC positioning during gantry rotation, dose delivery accuracy under different DR and GS conditions, and dose delivery accuracy for different combinations of MLC speed and DR. These procedures are stated by the authors to be "an initial attempt in designing a commissioning and QA protocol" and are subject to some limitations. Firstly, the synchronisation between the MLC, DR and gantry angle is not assessed and quantified within this set of tests.[11] As a result, no measurements are performed to verify that the

MLCs are at the correct position at the intended gantry angle or that the correct dose is delivered at the intended gantry angle. Secondly, due to the limitations associated with using integrated measurement devices (e.g. film or integrated MV images) the control systems cannot be assessed individually and hence their accuracy cannot be quantified in isolation. As a result, it is not possible to identify the source of any detected errors or monitor the performance of each control system separately over time.

Van Esch et al. [6] developed a set of tests which focused specifically on verifying that the monitor units (MU) and MLC positions are correctly synchronised with gantry angle. These tests utilise film placed trans-axially within a phantom positioned at the linac isocentre. Whilst these tests address some of the limitations associated with non-gantry resolved QA measurements, the use of film can be time consuming and labour intensive thereby limiting the ability to apply these procedures on a regular basis. Van Esch et al. also designed a more streamlined test which relies on a single integrated EPID image to assess the combined interplay between MLC position, dose delivery and gantry angle. While this test is time-efficient, it has the disadvantage that the performance of each control system is convolved into a single measurement, hence MLC and dose control cannot be assessed and monitored individually. Another disadvantage is that gantry angle synchronisation is not evaluated as the EPID rotates with the linac and images are averaged over large 90˚ arc segments.

A number of procedures have been proposed which rely on detector arrays within commercial QA phantoms for VMAT-specific linac QA.[12-14] Wang et al. developed a methodology which utilises a helical diode array and custom QA plan for routine linac QA.[14] This methodology was shown to be very efficient, however the use of diode array devices for this purpose is limited by the spatial resolution of the two-dimensional detector array, particularly for QA of the dynamic MLC. Barnes et al.[12, 13] developed methodologies for QA of DR and profile constancy as a function of gantry angle using time-resolved measurements from a 2D ion chamber array. The main disadvantage of this approach is that the same device cannot be used to assess MLC performance during VMAT due to the inadequate spatial resolution of the detector array. The authors also state that the use of a more

universally available and applicable device, such as the EPID, would be more suited to perform these procedures.

One popular approach to treatment delivery system quality control is the use of machine log files (e.g. Varian Dynalog files).[5, 15-22] Machine log files offer a number of advantages such as the ability to streamline and automate QA processes however, a number of recent studies have shown that log files are insensitive to some types of delivery errors.[16, 23, 24] This insensitivity arises from the fact that the parameters recorded by log files (i.e. MLC positions, gantry angle and dose fraction) are sourced from the linac control system itself and hence are not independent measurements. This was demonstrated by Agnew et al.[16] who showed that Varian Dynalog files were not sufficient to detect MLC leaf calibration errors and backlash. Similar observations were made by, Niel et al.[24] who reported on systematic differences between log file derived MLC positions and actual MLC positions greater than 1 mm during a clinical delivery.

The use of integrated EPID imaging for linear accelerator QA has a number of advantages, including high spatial resolution, large detector size and minimal setup time. EPID imaging is also available on all major commercially available linear accelerators and image acquisition can be easily automated within the treatment delivery system. Despite these clear advantages, integrated imaging is fundamentally limited as it cannot be used to directly measure the MLC positions, DR and GS as a function of time during the delivery. Accessing the individual EPID image frames, rather than a single integrated EPID image, allows direct measurement of these time-varying components without compromising the efficiency of the procedure. A number of groups have investigated the use of time-resolved EPID imaging for linac QA[25-31] and plan-specific QA[25, 32-36] for IMRT and VMAT deliveries. Zwan et al.[25] developed a system to automatically extract MLC trajectories from EPID image frames which could be subsequently compared to the planned MLC positions in order to calculate MLC positioning errors for each individual leaf as a function of gantry angle. This methodology was tested using clinical prostate and head and neck VMAT plans for plan-specific MLC QA but was not used in conjunction with a suitable QA test plan for linac QA purposes.

There is widespread consensus in the medical physics community that the available tests for VMAT-specific linac QA are insufficient resulting in a dependence on patient specific QA.[5, 6, 12-14, 25, 26, 36] Many of the challenges associated with quality control of VMAT are addressed in the most recent report from the Netherlands Commission on Radiation Dosimetry (NCS Report 24)[37], who make recommendations for VMAT-specific linear accelerator QA and commissioning. Since the release of this report, no work has been done to develop a single system which systematically addresses all of these recommendations.

The aim of this work is to develop a comprehensive and time-efficient system for commissioning and QA of VMAT delivery systems which assesses the performance of each individual dynamic machine component as a function of gantry angle. EPID image frames are acquired at 9.5 frames-per-second without the presence of a phantom during the delivery of a set of custom-designed QA test plans. From these acquired images, MLC positioning accuracy, dose delivery accuracy, profile constancy, DR constancy and GS constancy were assessed as a function of gantry angle. This QA methodology is independent of the delivery system as it relies solely on EPID images taken without a phantom or external detector. Image acquisition and analysis has been fully automated to streamline the QA procedure. This system has the ability not only to detect errors, but also to differentiate between each component of the delivery and determine at what point in the delivery the component failed. This work details the first set of procedures specifically designed to assess all components of VMAT deliveries as a function of gantry angle relying solely on time-resolved EPID imaging.

II. MATERIALS AND METHODS

II.A. Overview of method

The methodology developed for commissioning and QA of VMAT delivery systems can be summarised in Figure 1 below. This process includes (1) the delivery of 7 VMAT test plans, (2) acquisition of EPID image frames during these deliveries without the presence of a phantom, (3) automatic image analysis to directly measure dosimetric and MLC parameters and (4) comparison of measured parameters to the DICOM plan, machine log files and baseline data as a function of gantry angle.

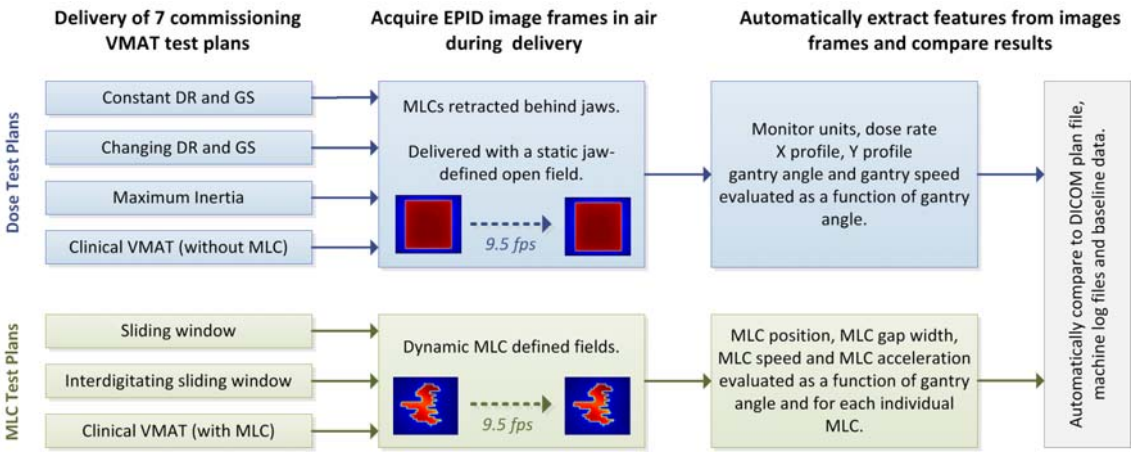

Figure 1: Overview of methodology developed for VMAT QA and commissioning.

II.B. Delivery systems and image acquisition

The procedures developed in this study were tested using a Varian 2100 IX linac (Varian Medical Systems, Palo Alto, CA) for a 6 MV photon beam. This treatment unit was equipped with a Millennium 120 leaf MLC which has a 5 mm and 10 mm leaf width for the central and outer leaves respectively. EPID images were collected using an aS1000 EPID which was operated in integrated mode and has a pixel size of 0.392×0.392 mm^2. All images were acquired with a source to detector distance (SDD) of 100 cm and were automatically flood field and dark field corrected. Individual EPID image frames were collected at a rate of 9.5 frames per second using an ancillary PC equipped with a dual-channel frame grabber system and in-house acquisition software. The gantry angle from the OBI gantry angle encoder was tagged to the header of each acquired image frame.[25, 36] The gantry angle naming convention used by this system and subsequently throughout this work, is $0^\circ = 0^\circ_{IEC}$, $90^\circ = 90^\circ_{IEC}$, $179^\circ = 179^\circ_{IEC}$, $-90^\circ = 270^\circ_{IEC}$ and $-179^\circ = 181^\circ_{IEC}$ relative to IEC 61217 (2008) scale.

II.C. Image analysis techniques

A set of test plans was designed to stress test various components of the delivery system during VMAT. Two categories of plans were created (1) dosimetry test plans and (2) MLC test plans. The dosimetry test plans rely on static jaw-defined fields without in-field MLC motion whilst the MLC test plans incorporated dynamic MLC trajectories.

II.C.1. Image analysis for dosimetry test plans

The following machine parameters were extracted from each individual EPID frame during delivery of the dosimetry test plans: MU, DR, X profile (transverse), Y profile (radial), gantry angle and GS.

The MU per frame was measured by calculating the average pixel value from the central 1×1 cm^2 region of the EPID. This was subsequently converted to MU using a pixel-to-MU conversion factor which was determined by delivering a 100 MU calibration field at 0˚ gantry angle with the same field size and SDD as the test plan deliveries. Equation 1 below details the conversion of the pixel values in each frame, S_{frame}, to MU where $S_{int,100MU}$ is the central axis pixel value for an integrated EPID image of a 100 MU delivery.

$$MU\ per\ frame = S_{frame} \times \left[\frac{100\ MU}{S_{int,100MU}}\right]$$

Using the MU per frame the cumulative MU could be calculated by summing the MU for all previous frames. The DR (in MU/min) per frame could then be determined using the known integration time of each image frame. The measured cumulative MU versus gantry angle was subsequently compared to the control points of the DICOM plan file for each test plan.

X and Y profiles through the central axis were also extracted from each EPID image frame. The beam profiles were averaged every 10 frames (approximately every second) and compared to baseline beam profiles acquired from a 100 MU integrated EPID image with a static gantry at 0˚. Off-axis ratios (OAR) for the central 80% of the field in the X and Y direction were used as the metric to compare the profiles at each gantry angle to the baseline. The maximum percentage change in any given X and Y off-axis ratio was reported as a function of gantry angle. Note that the 10-frame averaging was required as the EPID image is read out in the Y-direction as a function of time. Therefore, any rapid changes in DR during the readout of a single frame is reflected within the beam profile in the Y direction.[38] Averaging of 10 frames was chosen as a compromise to average out this effect without unnecessary reduction in the gantry angle resolution.

The GS was computed as a function of time during each delivery using the gantry angle and time stamp in the EPID image frame header.

II.C.2 Image analysis for MLC test plans

For each MLC test plan, the MLC positions were extracted from each EPID image frame using the methodology outlined in Zwan et al.[25] In this process, collimator rotation is removed and correction are made for MLC, gantry and image panel sag using a measured sag map in order to precisely extract the profile through the centre of each leaf pair. The radiation field edge can then be detected for each in-field MLC leaf and corrected for transmission through the curved leaf tip to give the light field edge position, i.e. the geometric leaf position[39] which is specified in the DICOM plan file.

Once the MLC positions were determined the MLC position error could be calculated for each individual MLC leaf as a function of gantry angle by comparing the measured MLC positions to the control points of the DICOM plan file. Note that the MLC control system attempts to produce linear MLC motion between control points[40] and so linear interpolation was used to determine the planned MLC positions at each EPID frame in between control points. Using the measured MLC positions from each frame, the leaf speed, leaf acceleration and leaf-pair gap error for each leaf could be calculated as a function of gantry angle.

II.D. Design of dosimetry test plans

Four dosimetry test plans were created with varying levels of delivery complexity. The specialized plans were constructed within MATLAB® (Mathworks, Natick, MA) by manually creating a set of control points within the DICOM plan structure. The created DICOM files were then imported as VMAT plans into the treatment planning system (TPS) so that the control system during the delivery was identical to a RapidArc patient treatment. Unless stated otherwise, dosimetry test plans were delivered with a static 25×25 cm^2 jaw-defined field with the MLCs retracted beyond the field edge. All dosimetry and MLC plans were constructed and delivered with both clockwise and counter-clockwise gantry rotation. From each of these test plans the cumulative MU, DR, beam profiles and

GS could be extracted as a function of gantry angle and compared to the planned values or to a baseline.

II.D.1 Dose Test 1: constant DR and GS

Dose Test 1 assesses the dosimetric performance of the delivery system during VMAT arcs with the lowest level of complexity, where both the GS and DR are constant throughout the delivery. The GS and DR were intentionally set to be at a maximum, i.e. 4.8 degrees per second and 600 MU/min respectively.

II.D.2 Dose Test 2: DR and GS transitions

Simultaneous changes in DR and GS were introduced into Dose Test 2 every 30˚ of gantry rotation. In regions between each transition the DR and GS were kept constant. This test allows calculation of the dosimetric performance for different combinations of constant DR and GS as well as in regions when these parameters are changing rapidly (Table 1). Note that there are no segments containing both low GS and low DR as the GS is only lowered when the DR is at a maximum.

Table 1: Planned GS and DR during 30˚ segments for clockwise delivery of Dose Test 2. Maximum and Low DR refers to 600 MU/min and 100 MU/min respectively and Maximum and Low GS refer to 4.8˚/s and 1.0˚/s respectively.

Arc Segment	GS	DR
-180˚→-150˚	Low	Maximum
-150˚→-120˚	Maximum	Low
-120˚→-90˚	Maximum	Maximum
-90˚→-60˚	Low	Maximum
-60˚→-30˚	Maximum	Low
-30˚→0˚	Maximum	Maximum
0˚→30˚	Low	Maximum
30˚→60˚	Maximum	Low
60˚→90˚	Maximum	Maximum
90˚→120˚	Low	Maximum
120˚→150˚	Maximum	Low
150˚→180˚	Maximum	Maximum

II.D.3 Dose Test 3: dose delivery with maximum inertia

Rapid transitions in GS can result in dose delivery errors, if gantry acceleration exceeds a threshold. Dose Test 3 was adapted from the Maximum Allowable Inertia Overshoot (MAIO) test suggested by the Netherlands Commission on Radiation Dosimetry (NCS Report 24).[37] This test is designed to deliver a VMAT arc with maximum changes in inertia of the gantry and simultaneous maximum changes in DR. This test plan was included, not as a representative of a clinical delivery, but as the most challenging delivery that could potentially be required by the treatment unit under any conditions.

II.D.4 Dose Test 4: clinical VMAT delivery

In addition to the test plans listed previously, a clinical VMAT delivery was also included within the test set. This plan comprises of a dual-arc head and neck VMAT treatment which is delivered with constant GS and typical DR modulation. The planned MLC positions for this plan were retracted such that all MLC motion occurred behind the jaw-defined 10×10 cm^2 static field. Note that each MLC leaf trajectory was not altered in this process, but was simply retracted by a constant amount at all control points so as not to obscure the jaw-defined static field.

II.E. MLC test plans

Three MLC test plans were specifically designed to evaluate the different aspects of the MLC control system. The complexity of the planned MLC trajectories was systematically increased for each test plan starting with simple sliding gap MLCs during arc rotation and building to a complex clinical VMAT delivery. For every MLC leaf of each test plan the MLC trajectory, positional error, gap error, leaf speed and leaf acceleration was measured as a function of gantry angle and compared to the planned MLC positions from the DICOM plan file. All plans were constructed with 0˚ collimator in order to assess the impact of gravity on MLC motion.

II.E.1 MLC Test 1: sliding window during gantry rotation

MLC Test 1 was designed to assess the dynamic MLC positioning accuracy for the simplest type of MLC motion, where there is no friction between adjacent leaves and no interdigitation. This test can be described as a series of arc segments where each segment contains a 2 cm sliding gap MLC pattern. The sliding gap motion of the MLC during each segment is depicted in Figure 2 (a) where all MLCs are moving in the same direction at the same speeds. Each segment contains the same sliding gap motion but with varying MLC speeds (ranging from 5 mm/s to 25 mm/s). The direction of MLC travel was reversed between each segment to allow bi-directional assessment of the MLCs acceleration (Table 2).

Table 2: Planned arc segment size, MU per segment and MLC speed for each segment of MLC Test 1. Planned MLC speeds were calculated assuming the dose is delivered at a maximum DR (600 MU/min) throughout the plan. Each MLC bank traversed 12 cm of motion within each arc segment. MLC motion during retraction was denoted as positive (+) MLC speed and MLC motion during extension was denoted as negative (-) MLC speed.

Gantry Angle Segment	Arc Segment Size	MU per Segment	Planned MLC Speed (mm/s)	
			Bank A	Bank B
176.8˚ → 119.2˚	57.6˚	240	+5	-5
119.2˚ → 61.6˚	57.6˚	240	-5	+5
61.6˚ → 42.4˚	19.2˚	80	+15	-15
42.4˚ → 23.2˚	19.2˚	80	-15	+15
23.2˚ → 8.8˚	14.4˚	60	+20	-20
8.8˚ → -5.6˚	14.4˚	60	-20	+20
-5.6˚ → -17.2˚	11.5˚	48	+25	-25
-17.2˚ → -28.6˚	11.5˚	48	-25	+25
-28.6˚ → -40.2˚	11.5˚	48	+25	-25
-40.2˚ → -51.7˚	11.5˚	48	-25	+25
-51.7˚ → -66.1˚	14.4˚	60	+20	-20
-66.1˚ → -80.5˚	14.4˚	60	-20	+20
-80.5˚ → -99.7˚	19.2˚	80	+15	-15
-99.7˚ → -118.9˚	19.2˚	80	-15	+15
-118.9˚ → -147.7˚	28.8	120	+10	-10
-147.7˚ → -176.5˚	28.8	120	-10	+10

II.E.2 MLC Test 2: interdigitating sliding window during gantry rotation

MLC Test 2 assesses the dynamic MLC performance with interdigitation. This test contains the same MLC trajectories, speeds and acceleration as in MLC Test 1 (see Table 2) but with alternating (odd/even) MLC leaves always travelling in opposite direction as depicted in Figure 2. This test was designed to simulate the highest amount of friction between adjacent MLC leaves during interdigitation. As with MLC Test 1 this plan incorporates a range of MLC speeds, assesses motion in both directions and includes changes in direction of travel between each segment.

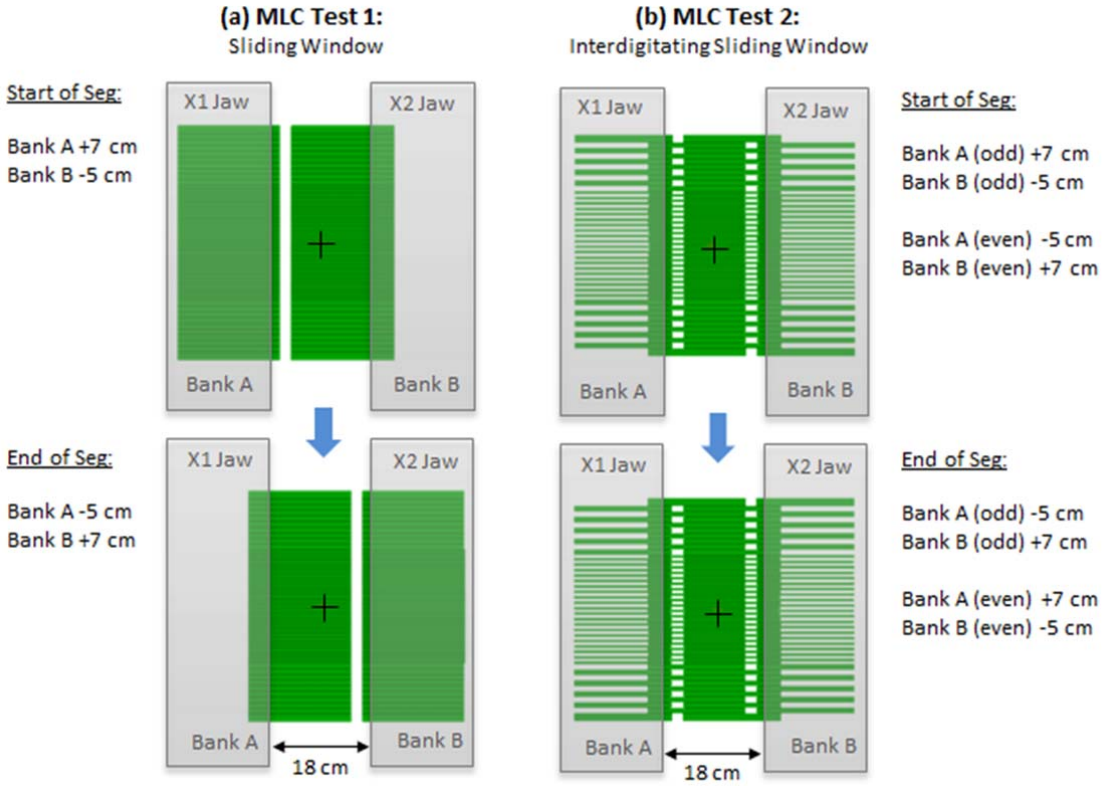

Figure 2: Visual representation of MLC positions at the start and end of each arc segment for (a) MLC Test 1: sliding window and (b) MLC Test 2: interdigitating sliding window. The trajectories are repeated in different segments using varying MLC speeds and direction of MLC motion as described in Table 2.

II.E.3 MLC Test 3: clinical VMAT delivery

MLC performance during a dual-arc clinical Head and Neck VMAT plan was also evaluated. This test is limited in that it does not assess accuracy of all MLC leaves equally, however, it does provide an overall assessment of the MLC control system during an actual clinical delivery which incorporates changes in DR, a range of MLC speeds and accelerations, varying gap widths and collimator rotation.

II.F. Machine log file analysis

Machine log files (Varian Dynalog files) were also obtained during the delivery of each dosimetry and MLC test plan in order to compare the EPID-measured parameters with those recorded by the linac control system.

For the dosimetry test plans, the gantry angle, GS, DR and cumulative MU were extracted at 50 ms intervals from the log files. As dose fraction is recorded in the log file rather than the absolute dose output, the dose fraction was subsequently converted to absolute DR and cumulative MU by assuming the correct total MU was delivered. Note that, in order for the linac to record Varian Dynalog files some MLC motion is required. To enable the acquisition of Dynalog files for the dosimetry plans (where there is no MLC motion within the field) a single MLC was moved behind the jaws during the delivery.

For the MLC test plans, the MLC positions were extracted and compared to the corresponding EPID-measurements and the planned MLC positions. All log file MLC positions were post-processed to remove the leaf position offset (LPO) correction prior to any comparisons.[25, 39]

II.G. Clinical implementation

All test plans used in this study were imported into a single QA patient within an Eclipse TPS (Version 11.031, Varian Medical Systems) and delivered in clinical mode. An in-house software tool was developed using MATLAB® to automatically analyse the acquired data, compare the measurements to the DICOM plan file and save the results in graphical and quantitative format. This tool was equipped with a graphical user interface which was designed to streamline the QA process.

III. RESULTS

III.A. Dosimetry test results

III.A.1 Output verification during VMAT

Figure 3 shows the measured error in relative dose delivered as a function of gantry angle for (a) Dose Test 1, (b) Dose Test 2, (c) Dose Test 3 and (d) Dose Test 4. Percentage errors were computed by comparing the MU measured from EPID images (MU_{Meas}) to the MU from the DICOM plan file (MU_{Plan}). The relative dose error at each gantry angle in Figure 3 is defined as $100 \times [MU_{Meas} - MU_{Plan}]/MU_{Total}$, where MU_{Total} is the total cumulative MU for the arc. The largest relative dose error at any gantry angle was 0.8% for the Maximum Inertia test (see Figure 3 (c)) and 0.25% for all other tests. The same analysis was performed using fractional dose recorded by log files. In Dose Test 2, a 1˚ synchronisation error between the linac output and gantry angle was introduced by editing the planned control points from 60˚ to 180˚.

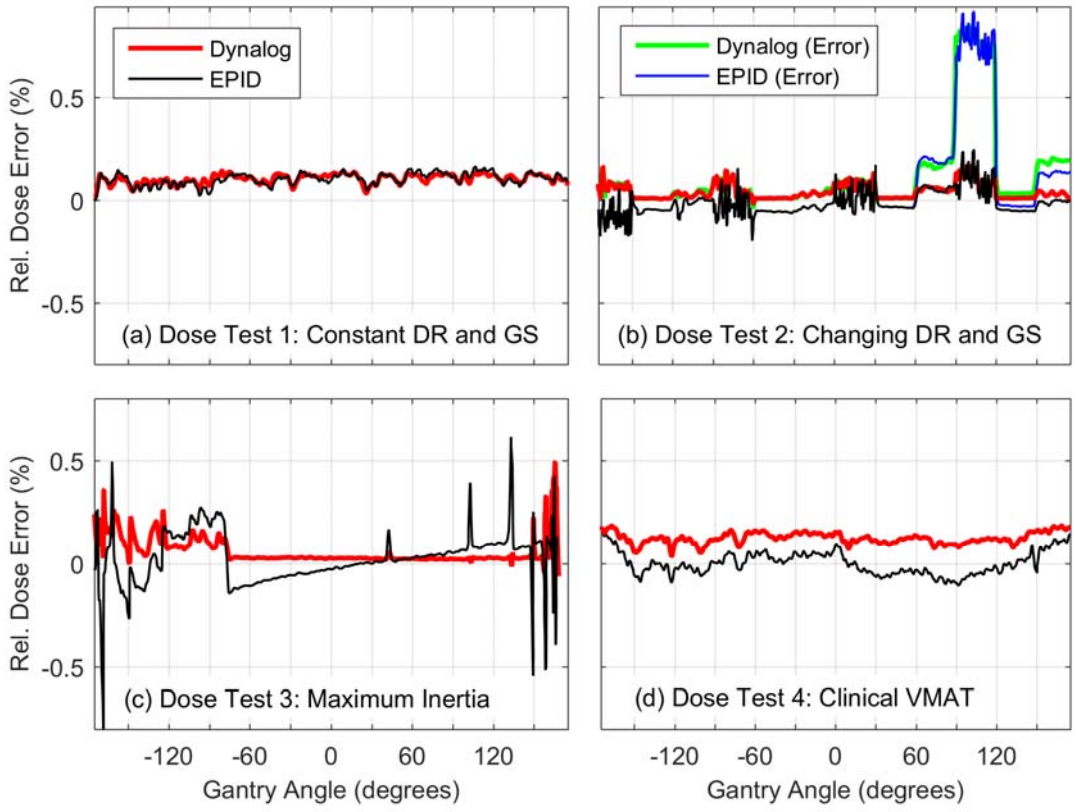

Figure 3: Relative dose error as a function of gantry angle computed using time-resolved EPID imaging and Dynalog files for the same delivery of (a) Dose Test 1, (b) Dose Test 2, (c) Dose Test 3 and (d) Dose Test 4. Each of these plans consist of both clockwise and counter-clockwise arcs, however, this figure only gives results for the clockwise case for clarity.

III.A.2 DR and GS during VMAT

Figure 4 shows an example of the DR and GS as a function of gantry angle for Dose Test 3. Measurements of DR and gantry angle are given using both the EPID and log files.

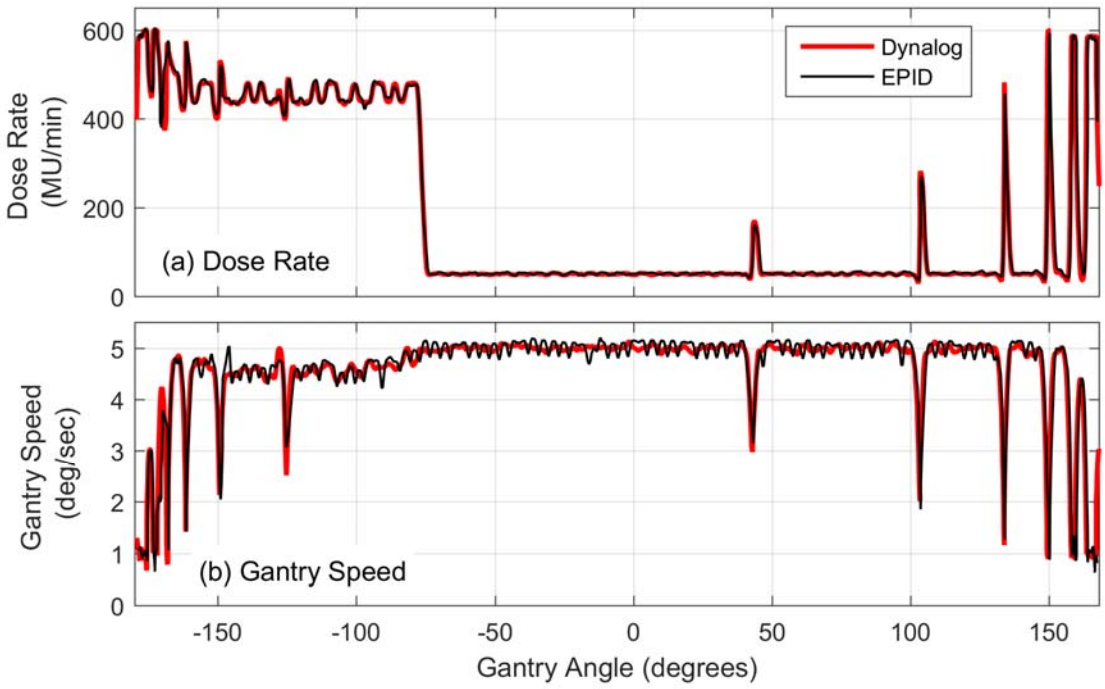

Figure 4: Example of measured (a) DR and (b) GS during the clockwise arc of Dose Test 3: maximum inertia. Results are plotted based on EPID imaging and Dynalog files.

III.A.3 Beam profile constancy during VMAT

The maximum change in OAR (OAR_{max}) in the X and Y direction was measured as a function of gantry angle for all test plans. Figure 5 (a) and (c) shows the X and Y OAR_{max} versus gantry angle for Dose Test 1 where each data point represents the average of 10 image frames. Similarly, Figure 5 (b)

and (d) gives a plot of the X and Y OAR_{max} for Dose Test 2. Here each point represents the average profile of all images in each 30˚ arc segment, where each 30˚ segment of the plan contains a different combination of DR and GS as detailed in Table 1. The data points contained within the dashed circles correspond to segments where the nominal DR was at a minimum and the GS was at a maximum (see Table 1).

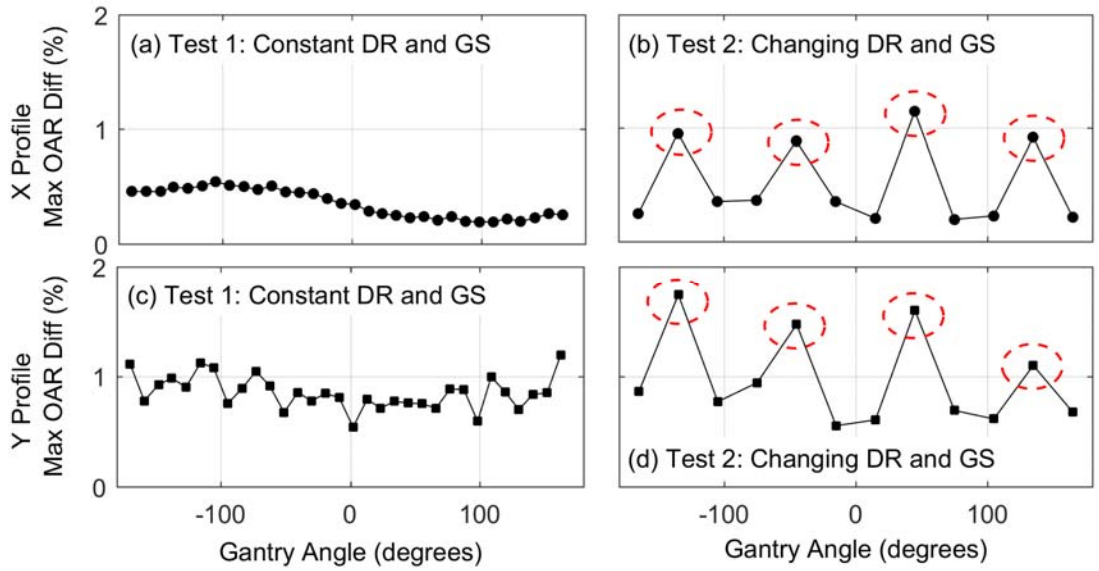

Figure 5: Maximum difference in OAR as a function of gantry angle for X and Y beam profiles. Results are given here for Dose Test 1 ((a) and (c)) where the DR and GS are constant and Dose Test 2 ((b) and (d)) where the DR and GS were changed every 30˚.

III.B. MLC Test Results

III.B.1. MLC positioning accuracy

The overall MLC positional accuracy during the delivery of each dynamic MLC test plan is summarised in Figure 6, which shows a histogram of the differences between the planned and measured MLC positions for MLC Test 1, 2 and 3. The histograms include all MLC leaves and both clockwise and counter-clockwise deliveries of each test.

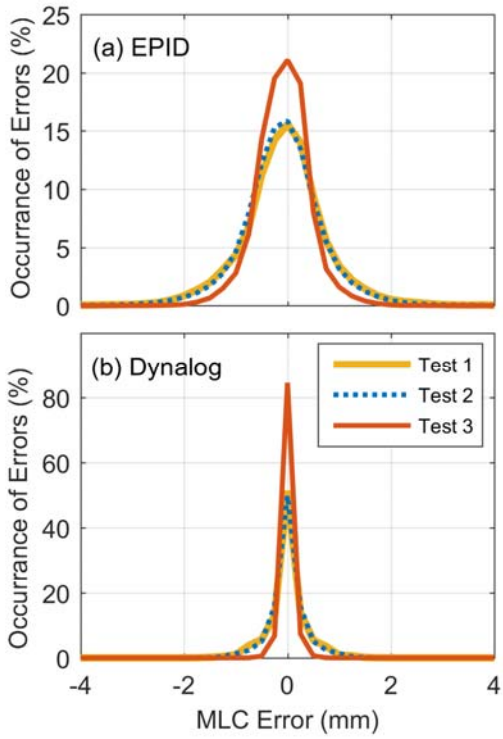

Figure 6: Histogram of differences between the planned MLC positions and (a) EPID measurements and (b) Dynalog files for MLC Test 1: sliding window, MLC Test 2: interdigitating sliding window and MLC Test 3: clinical VMAT. A 0.25 mm bin-width was use to partition the data.

To assess the performance of each MLC leaf individually, the mean error and standard deviation of the error was computed on a leaf-by-leaf basis for each test plan. Figure 7 shows the positional error measured for each leaf in MLC Tests 1, 2 and 3. Each point represents the mean of the difference between the measured MLC position and the planned MLC position averaged over the entire arc. The error bars in the plot represent the standard deviation of this difference. Each plan comprised of arcs with both clockwise and counter-clockwise gantry rotation, however, only the clockwise case for MLC bank A is shown here for simplicity. To demonstrate the sensitivity of this methodology MLC errors were simulated in MLC Test 1 (Figure 7 (a)) for leaf 20A and 40A corresponding to systematic and random errors respectively of magnitude 1 mm. These errors were simulated by manually editing the MLC positions in the DICOM plan file.

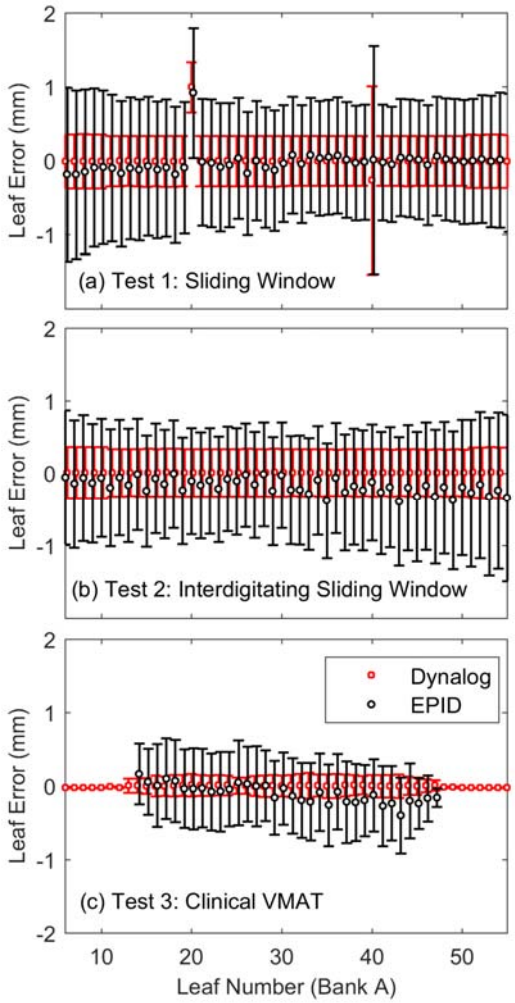

Figure 7: The mean and standard deviation of MLC positional error for each leaf of MLC Bank A for the clockwise delivery of (a) MLC Test 1: sliding window, (b) MLC Test 2: interdigitating sliding window and (c) MLC Test 3: clinical VMAT. Errors were computed based on both EPID and Dynalog files. Systematic and random position errors were respectively introduced into leaf A20 and A40 respectively of MLC Test 1.

III.B.2. MLC gap accuracy

MLC gap accuracy was also specifically assessed for each individual MLC leaf-pair. Figure 8 (a), (b) and (c) show the measured mean and standard deviation of the MLC gap errors for the clockwise delivery of MLC test 1, 2 and 3 respectively. The analysis was performed using measured MLC positions from EPID images and recorded MLC positions from machine log files. MLC gap errors

were introduced into leaf-pair 21 and 41 of the DICOM plan with a magnitude of 0.4 mm and 0.6 mm respectively for MLC Test 1.

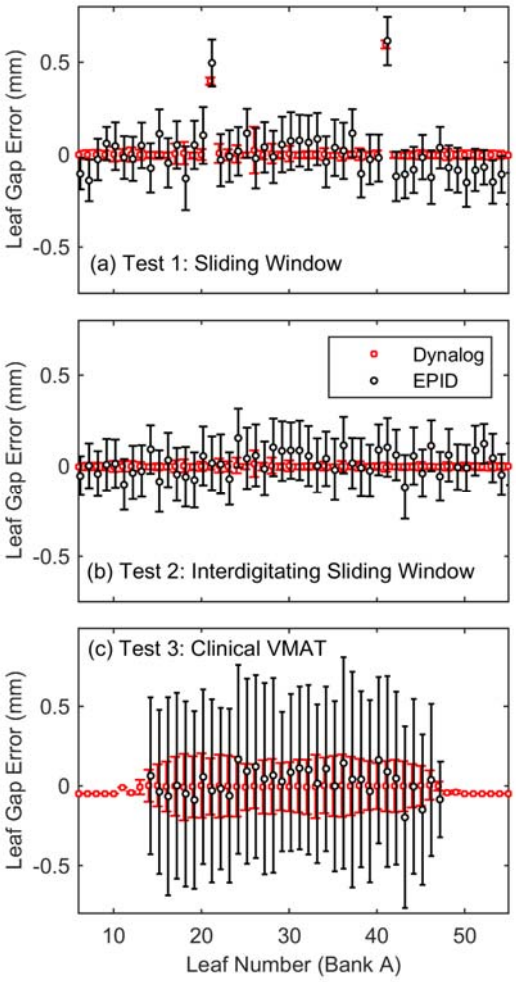

Figure 8: The mean and standard deviation of the MLC gap error for each leaf of MLC Bank A for the clockwise delivery of (a) MLC Test 1: sliding window, (b) MLC Test 2: interdigitating sliding window and (c) MLC Test 3: clinical VMAT. Systematic MLC gap errors were introduced into MLC Test 1.

III.B.3. Synchronisation between MLC and gantry angle

MLC performance was also investigated as a function of gantry angle during the delivery of each test plan. Figure 9 shows a plot of the mean MLC positioning error at each gantry angle averaged over all in-field MLCs for MLC Test 1. For this delivery a synchronisation error of 0.5˚ was simulated by

editing the control points of the plan for all control points in the second half of the arc (i.e. from 0˚ to -180˚).

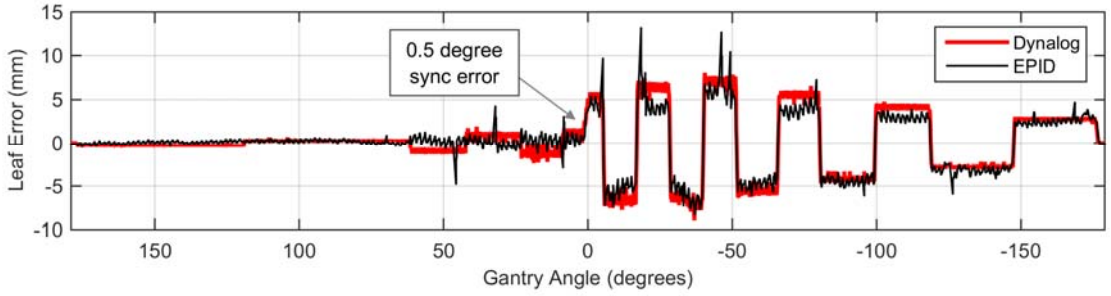

405

Figure 9: Mean MLC positioning error at each gantry angle for counter-clockwise delivery of MLC Test 1 as measured using the EPID and recorded in Dynalog files. For this test a synchronisation error was introduced mid-way through the arc.

III.B.4. MLC speed and acceleration constancy

410 As described in Table 2, MLC leaves were driven at a range of constant speeds during gantry rotation within MLC Test 1 and 2. Figure 10 shows an example of the measured MLC speed for each leaf during arc segments with nominal speeds of (a) 5 mm/s, (b) 15 mm/s and (c) 25 mm/s. For each MLC leaf, speeds were measured using EPID images and calculated from log files. Note that only Bank A MLCs for a single clockwise delivery are given in Figure 10 as a representative sample of the results.

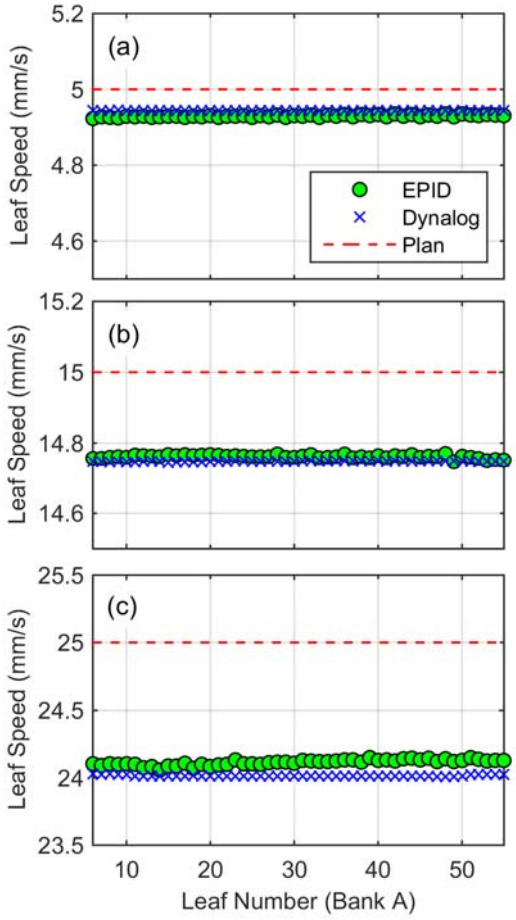

Figure 10: EPID-measured and Dynalog-recorded MLC speed for each individual MLC leaf for 3 segments of MLC Test 1 – sliding window during gantry rotation. Plots (a), (b) and (c) correspond to different segments of the plan with nominal MLC speeds of 5, 15 and 25 mm/s respectively.

The planned MLC speed within each plot of Figure 10 was computed assuming the DR was at a maximum of 600 MU/min during the delivery of each segment (see table 2). Figure 11 shows the actual mean DR within each segment (extracted from the log files). The figure also includes a "predicted dose rate" which was calculated from the difference between the measured and nominal MLC speed.

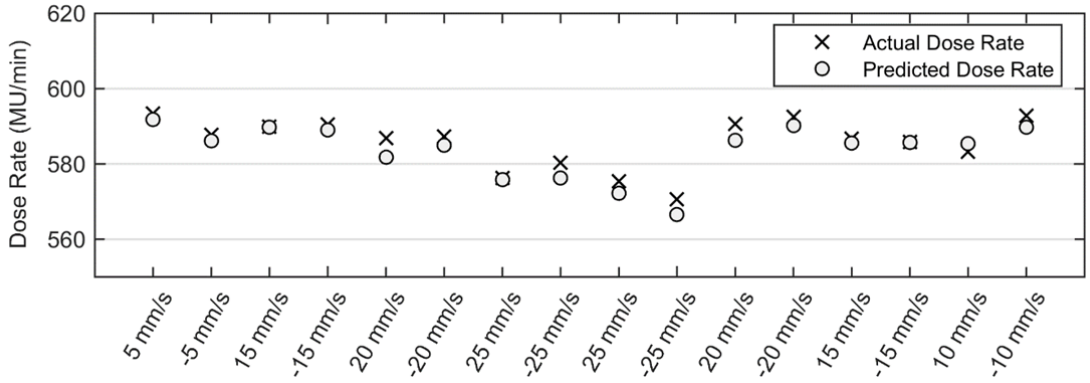

425 **Figure 11:** The mean DR for each segment of MLC Test 1 computed using the dose fraction from Dynalog files. The predicted DR is also plotted which was computed using the difference between the nominal MLC speed and the mean measured MLC speed during each segment. The x-labels represent the nominal MLC speed during each of the 16 segments of MLC Test 1: sliding window with gantry rotation (see Table 2).

430 IV. DISCUSSION

Accurate dose delivery during VMAT requires precise control of GS, DR and MLC positioning as a function of time. A comprehensive QA program should assess not only the performance of each control system in isolation, but also the synchronisation between each dynamic component. In this study a set of test deliveries and procedures were developed to measure the following parameters as a 435 function of gantry angle: dose delivery accuracy, DR constancy, beam profile constancy, GS constancy, dynamic MLC positioning accuracy, MLC speed and acceleration constancy, and synchronisation between gantry angle, MLC and dose. Each of these parameters was assessed during the delivery of a number of specially designed VMAT test plans each containing a different level of delivery complexity.

440 QA procedures developed in the past have focused on more of an overall assessment of VMAT where each test relies on the accuracy of more than one control system.[5, 6, 41] This approach is likely to be due to the inability of available QA devices to perform time-resolved measurements with a high spatial resolution. In this work, our approach has been to use time-resolved EPID imaging to isolate

each control system of the delivery (e.g. DR, GS, MLC position and beam profile) and to evaluate each component individually. This enables more informative QA procedures where there is no ambiguity as to the source of any detected errors. Assessment of each VMAT control system in isolation is also recommended in NCS Report 24 which states: "Since the dynamic behaviour includes gantry and MLC motion and DR variation, tests are needed to verify each quantity separately as well as combined".[37]

IV.A. Output verification during VMAT

The dosimetric accuracy of the delivery was evaluated during constant DR and GS (Dose Test 1), changing DR and GS (Dose Test 2), maximum inertia (Dose Test 3) and clinical VMAT conditions (Dose Test 4). Figure 3 indicates that increasing the complexity of the delivery results in larger errors in the dose. This is particularly evident for Dose Test 3 (i.e. the maximum inertia test), where cumulative dose errors greater than 0.5% are observed intermittently at some gantry angles. For all other test plans EPID and log file-based dose measurements agree with the planned dose within ±0.25% for all gantry angles. During Dose Test 2 (see Figure 3 (b)) regions of lower dose stability are observed in some segments. Table 1 shows that these segments are delivered with low GS and maximum DR indicating that the dose control system is less accurate for this combination of DR and GS.

A systematic offset of approximately ~0.1% was observed between EPID and log file-based dose measurements for Dose Test 2 and 4. The cause of this offset may be due to the fact that only a relative dose fraction is recorded in the log files, in contrast to the EPID-measured dose which is converted to absolute MU using a calibration image. Some other potential causes of this small offset are EPID imaging artefacts such as gain-ghosting, image lag and DR dependence. The time-varying DR and GS were plotted individually for Dose Test 3 (see Figure 4) to determine the source of the observed dose errors. Figure 4 shows that the dose errors correspond to synchronised rapid changes in both GS and DR, which indicates that the errors may be due to inertia of the gantry. At these points in the delivery, the gantry is required to change velocity faster than possible which results in a transient

dosimetric error as seen in Figure 3(c). This example illustrates the advantages of directly measuring each individual component of the delivery so that the source of dose discrepancies can be determined.

The QA procedures were found to be sensitive to simulated errors as seen in Figure 3 (b) where a 1˚ synchronisation offset was introduced into Dose Test 2. This type of error was chosen as it illustrates the sensitivity of this method to gantry angle synchronisation errors which may not be detected by traditional QA procedures which rely on integrated EPID imaging or film measurements.[11] An example of such a test is the popular Ling Test 2,[5] where integrated dose is assessed and no measurement is performed to ensure the dose is delivered at the correct gantry angle. Note that, the magnitude of the simulated errors (both MLC and dose) approximate the minimum detectable error using this system.

IV.B. Beam profile constancy during VMAT

Profile constancy was assessed as a function of gantry angle. The EPID-measured profiles were not directly related to the actual beam profile flatness and symmetry in water, due to off-axis energy response and the nature of the flood-field correction.[42] Rather, the profiles measured at each gantry angle were compared to baseline profiles at gantry 0˚ using an off-axis ratio (OAR) as suggested in AAPM TG 142.[43] Dose Test 1 (Figure 5 (a) and (c)) indicates that there is no substantial variation in profile constancy as a function of gantry angle for deliveries where the GS and DR was constant. Dose Test 2 (Figure 5 (b) and (d)) shows that beam profiles were found to be less stable in segments with low DR and high GS compared to other segments. Note that, the accuracy of X profile measurements using the EPID is extremely high due to the fast readout time of each row of the imager, high spatial resolution and high reproducibility of each pixel response. For the Y profile, rapid changes in dose rate can reduce the accuracy of the measurement as discussed in section II.C.1.

IV.C. MLC positioning accuracy

MLC positioning accuracy was measured for dynamic MLCs under a range of conditions. In terms of the overall leaf positioning accuracy, no differences were observed between sliding gap MLC patterns

with and without friction/interdigitation (see Figure 6). In general, leaf positioning during the clinical VMAT delivery (MLC Test 3) was found to be more accurate than the test patterns in MLC Test 1 and 2. This is expected as these tests were designed to represent the most complex MLC trajectories (in terms of speed and acceleration) that could occur in a clinical plan.

The performance of each individual MLC leaf was evaluated using the mean and standard deviation of the MLC positioning error averaged over the entire arc (see Figure 7). Simulated errors in leaf 20A and 40A for MLC Test 1 show that this methodology is capable of detecting single MLC leaf errors as small as 1 mm and can be used to determine the type (e.g. random or systematic) and magnitude of detected errors. The types of MLC errors simulated were chosen as they represent realistic clinical MLC positioning errors which have been demonstrated by other groups,[16, 24] for example MLC calibration errors (systematic offsets) and MLC motor failures (random positioning errors).

IV.D. MLC gap accuracy

In addition to mean positioning error, leaf gap errors were also measured for each MLC of each test plan as shown in Figure 8. A larger deviation in gap error was seen for the clinical delivery (MLC Test 3), where gap between opposing leaf-pairs is changing rapidly, compared to MLC Test 1 and 2, where the gap is fixed during the delivery. MLC gap errors were simulated in MLC Test 1 and detection and classification of errors as small as 0.4 mm was demonstrated (see Figure 8 (a)). Note that, the reason for specifically assessing the average gap error for each leaf pair is that these types of errors have been shown to produce the largest systematic dose delivery errors during clinical VMAT deliveries.[44]

IV.E. Synchronisation between MLC and gantry angle

MLC performance was also assessed as function of gantry angle to identify any gantry angle dependency and detect synchronisation errors between the MLC and gantry angle control systems. Figure 9 shows the mean MLC positioning error versus gantry angle averaged over all MLC leaves for MLC Test 1. For this example, a synchronisation error between MLC and gantry angle of 0.5˚ was

introduced at 0˚ to -180˚. An error such as this could not be detected using traditional MLC QA procedures for VMAT, for example the picket fence test proposed by Ling et al.[5] which was not designed to determine whether MLCs reach the correct position at the desired gantry angle.[11] Another limitation of the picket fence test proposed by Ling et al. is that the MLC trajectories are less complex than those present in a typical clinical VMAT plan. Firstly, the MLCs are static when forming the "pickets" in the integrated image which means that only static MLC positioning accuracy is evaluated. Secondly, the test does not incorporate any changes in direction during gantry rotation which is an additional complexity in VMAT compared to IMRT and should be specifically assessed.

It can also be observed that there is a difference between the mean errors measured by the EPID and by the Dynalog, particularly on the range of 0-60˚. These differences are due to the method for assigning a gantry angle from the OBI system to each EPID. As the MV and OBI systems operate at different frame rates this translates into a sampling error in the gantry angle and produces the oscillation seen in the EPID-measured leaf accuracy in Figure 9 which is accentuated on the range of 0-60˚ when the MLC speed is high.

IV.F. MLC speed and acceleration constancy

MLC speed constancy was addressed within MLC Test 1 and 2 by driving MLC leaves at five different constant speeds during segments of each arc delivery. Figure 10 shows an example of the measured MLC speed using EPID and log files for each MLC compared to the nominal speed for three of these segments during MLC Test 1. Both log files and EPID measurements indicate that the MLCs are travelling slower than their desired speed for all segments. This may result in a dosimetric error if the slower MLC speeds are not compensated for by lower DR s. A "predicted dose rate" could be computed using the difference between the nominal and measured MLC speed, which is the DR required to compensate for the slower MLC speeds in each segment. In Figure 11, this "predicted dose rate" is compared to the "actual dose rate" from log files for each segment. Figure 11 shows that in segments where the average DR is lower than the nominal DR of 600 MU/min (for example 570

MU/min in segment 10) the MLC speed is also lowered by the control system to a speed that would ensure the correct dose is delivered.

For all dosimetry and MLC tests, there was no significant difference in machine performance observed between clockwise and counter-clockwise rotations.

IV.G. Time efficiency and limitations

As treatment techniques increase in complexity, the required time and operational costs of additional quality management procedures also increases. This is discussed in the report from AAPM TG40[45] and more recently in AAPM TG100.[46] The latter report states that "labour intensive activities place a heavy demand on medical physicists" and that "mental and physical overload have been linked to serious errors in many radiation therapy related incidents and accidents". While it is ideal to perform QA tests that are comprehensive and of the highest standards, this must be balanced with the additional time and resources required to correctly and competently perform each test. Automation of modern QA techniques is paramount to achieving this balance in order to reduce the excessive demands on physics resources resulting from the increasing number and intensity of recommended QA tests. In this work, the deliveries are performed without the presence of a phantom which eliminates setup time and the analysis of acquired data is completely automated. The delivery of the test suite, which was designed as a commissioning or annual set, can be performed within 1 hour including setup time, calibration images and repeated clockwise and counter-clockwise deliveries. The efficiency of this process is a clear advantage over other more labour intensive QA methodologies for example those which rely on film or detector array measurements within a phantom.

A potential limitation in the use of EPID image frames acquired using the frame grabber, is the reliance on the gantry angle from the header of the EPID images. In this method, the header gantry angle is read out from the on-board OBI system and so is not entirely independent of the linac. Therefore, this gantry angle should not be relied on for QA purposes without being independently verified. The authors recommend that the EPID header gantry angle be compared to an independent

gantry angle measurement on a regular basis to ensure it is a true indication of the correct gantry angle. This may be done using one of the many available dynamic gantry angle measurement tools[27, 30, 47] or manually using a level as part of a regular quality control program.

II.H. Machine log file analysis

In general, measurements performed by the EPID agreed with information recorded by the machine log files. The EPID-measured parameters gave a larger standard deviation in errors when compared to log files however the mean errors were comparable.

Despite the lower standard deviation of log files and the reasonable agreement with EPID in this study, it is not recommended to rely solely on log files as the readout is sourced directly from the linac control system. In particular, care should be taken when using log files for MLC QA as the positions recorded may not reflect the actual location of the MLCs as other authors have demonstrated. [16, 23, 24] Note that in this study the log file analysis appeared to be sensitive to delivery errors introduced into Dose Test 2 and MLC Test 1, however this is due to the fact that errors were introduced into the DICOM plan file rather than the MLC, gantry angle or dose calibration. As the EPID measurements are a direct independent measurement of the MLC-defined radiation field and output they are not subject to the same inadequacies as log files and may be used as a gold standard for both MLC and dose delivery accuracy.

V. CONCLUSION

A set of VMAT test plans and analysis software has been developed to systematically assess the performance of all components of VMAT deliveries individually and as a function of gantry angle. The procedures have been shown to be sensitive to a range of delivery errors including random and systematic MLC errors, dose output errors and synchronisation errors. The methodology relies solely on time-resolved EPID imaging without the presence of a phantom and analysis of acquired image data was fully automated. The procedures developed in this work are both comprehensive and time-efficient and can be used for streamline gantry-resolved commissioning and QA of VMAT delivery systems.

VI. ACKNOWLEDGEMENTS

The authors wish to acknowledge Shashank Bhatia for development of the frame grabber acquisition software used to read and record image frame data from the electronic portal imaging device.

REFERENCES

[1] C. Yu, "Intensity-modulated arc therapy with dynamic multileaf collimation: An alternative to tomotherapy," Physics in Medicine and Biology **40**, 1435-1449 (1995).

[2] K. Otto, "Volumetric modulated arc therapy: IMRT in a single gantry arc," Medical Physics **35**, 310-317 (2008).

[3] P. Xia, L.J. Verhey, "Multileaf collimator leaf sequencing algorithm for intensity modulated beams with multiple static segments," Med Phys **25**, 1424-1434 (1998).

[4] D.A. Palma, W.F. Verbakel, K. Otto, S. Senan, "New developments in arc radiation therapy: a review," Cancer treatment reviews **36**, 393-399 (2010).

[5] C.C. Ling, P. Zhang, Y. Archambault, J. Bocanek, G. Tang, T. LoSasso, "Commissioning and quality assurance of RapidArc radiotherapy delivery system," Int J Radiat Oncol Biol Phys **72**, 575-581 (2008).

[6] A. Van Esch, D.P. Huyskens, C.F. Behrens, E. Samsøe, M. Sjölin, U. Bjelkengren, D. Sjöström, C. Clermont, L. Hambach, F. Sergent, "Implementing RapidArc into clinical routine: a comprehensive program from machine QA to TPS validation and patient QA," Medical Physics **38**, 5146-5166 (2011).

[7] M. Jørgensen, L. Hoffmann, J.B. Petersen, L. Praestegaard, R. Hansen, L. Muren, "Tolerance levels of EPID-based quality control for volumetric modulated arc therapy," Medical Physics **38**, 1425-1434 (2011).

[8] A. Manikandan, B. Sarkar, R. Holla, T. Vivek, N. Sujatha, "Quality assurance of dynamic parameters in volumetric modulated arc therapy," Br J Radiol. **85**, 1002-1010 (2012).

[9] Y.-C. Huang, C.-Y. Yeh, J.-H. Yeh, C.-J. Lo, P.-F. Tsai, C.-H. Hung, C.-S. Tsai, C.-Y. Chen, "Clinical practice and evaluation of electronic portal imaging device for VMAT quality assurance," Medical Dosimetry **38**, 35-41 (2013).

[10] A. Fogliata, A. Clivio, P. Fenoglietto, J. Hrbacek, S. Kloeck, P. Lattuada, P. Mancosu, G. Nicolini, E. Parietti, G. Urso, "Quality assurance of RapidArc in clinical practice using portal dosimetry," Br J Radiol. **84**, 534-45 (2011).

[11] A. Mans, D. Schuring, M.P. Arends, C.A. Vugts, J.W. Wolthaus, H.T. Lotz, M. Admiraal, R.J. Louwe, M.C. Öllers, J.B. van de Kamer, "The NCS code of practice for the quality assurance and control for volumetric modulated arc therapy," Physics in Medicine and Biology **61**, 7221 (2016).

[12] M.P. Barnes, P.B. Greer, "Time-resolved beam symmetry measurement for VMAT commissioning and quality assurance," Journal of Applied Clinical Medical Physics **17**, 220-30 (2016).

[13] M.P. Barnes, P. Rowshanfarzad, P.B. Greer, "VMAT linear accelerator commissioning and quality assurance: dose control and gantry speed tests," Journal of Applied Clinical Medical Physics **17**, 246-261 (2016).

[14] Q. Wang, J. Dai, K. Zhang, "A novel method for routine quality assurance of volumetric-modulated arc therapy," Medical Physics **40**, 101712 (2013).

[15] E. Schreibmann, A. Dhabaan, E. Elder, T. Fox, "Patient-specific quality assurance method for VMAT treatment delivery," Medical Physics **36**, 4530-4535 (2009).

[16] A. Agnew, C. Agnew, M. Grattan, A. Hounsell, C. McGarry, "Monitoring daily MLC positional errors using trajectory log files and EPID measurements for IMRT and VMAT deliveries," Physics in Medicine and Biology **59**, N49 (2014).

[17] C.D. Venencia, P. Besa, "Commissioning and quality assurance for intensity modulated radiotherapy with dynamic multileaf collimator: experience of the Pontificia Universidad Católica de Chile," Journal of Applied Clinical Medical Physics **5**, 37-54 (2004).
[18] D.W. Litzenberg, J.M. Moran, B.A. Fraass, "Incorporation of realistic delivery limitations into dynamic MLC treatment delivery," Med Phys **29**, 810-820 (2002).
[19] P. Zygmanski, J.H. Kung, S.B. Jiang, L. Chin, "Dependence of fluence errors in dynamic IMRT on leaf-positional errors varying with time and leaf number," Med Phys **30**, 2736-2749 (2003).
[20] A.M. Stell, J.G. Li, O.A. Zeidan, J.F. Dempsey, "An extensive log-file analysis of step-and-shoot intensity modulated radiation therapy segment delivery errors," Medical Physics **31**, 1593-1602 (2004).
[21] M. Okumura, Y. Obata, K. Shimomura, M. Tamura, Y. Nishimura, "The effect of gantry and collimator angles on leaf limited velocity and position in dynamic multileaf collimator intensity-modulated radiation therapy," Physics in Medicine and Biology **55**, 3101 (2010).
[22] V. Chandraraj, S. Stathakis, R. Manickam, C. Esquivel, S.S. Supe, N. Papanikolaou, "Consistency and reproducibility of the VMAT plan delivery using three independent validation methods," Journal of Applied Clinical Medical Physics **12**, 129-140 (2010).
[23] B.J. Zwan, J. Hindmarsh, E. Seymour, K. Kandasamy, K. Sloan, R. David, C. Lee, "The dosimetric impact of control point spacing for sliding gap MLC fields," Journal of Applied Clinical Medical Physics **17,** 204-216 (2016).
[24] B. Neal, M. Ahmed, K. Kathuria, T. Watkins, K. Wijesooriya, J. Siebers, "A clinically observed discrepancy between image-based and log-based MLC positions," Medical Physics **43**, 2933-2935 (2016).
[25] B.J. Zwan, M.P. Barnes, T. Fuandrod, S.C. J., D.J. O'Connor, P.J. Keall, P.B. Greer, "An EPID-based system for gantry resolved MLC quality assurance for VMAT," Journal of Applied Clinical Medical Physics **17**, 1-18 (2016).
[26] M. Bakhtiari, L. Kumaraswamy, D.W. Bailey, S. de Boer, H.K. Malhotra, M.B. Podgorsak, "Using an EPID for patient-specific VMAT quality assurance," Medical Physics **38**, 1366-1373 (2011).
[27] P.M. McCowan, D.W. Rickey, P. Rowshanfarzad, P.B. Greer, W. Ansbacher, B.M. McCurdy, "An investigation of gantry angle data accuracy for cine-mode EPID images acquired during arc IMRT," Journal of Applied Clinical Medical Physics **15**, 187-201 (2014).
[28] T. Fuangrod, P. Rowshanfarzad, P.B. Greer, R.H. Middleton, "A cine-EPID based method for jaw detection and quality assurance for tracking jaw in IMRT/VMAT treatments," Physica Medica **31**, 16-24 (2015).
[29] P. Rowshanfarzad, M. Sabet, D.J. O'Connor, P.M. McCowan, B.M. McCurdy, P.B. Greer, "Detection and correction for EPID and gantry sag during arc delivery using cine EPID imaging," Medical Physics **39**, 623-635 (2012).
[30] P. Rowshanfarzad, M. Sabet, D.J. O'Connor, P.M. McCowan, B.M. McCurdy, P.B. Greer, "Gantry angle determination during arc IMRT: evaluation of a simple EPID-based technique and two commercial inclinometers," Journal of Applied Clinical Medical Physics **13**, 203-214 (2012).
[31] B.J. Zwan, B.W. King, D.J. O'Connor, P.B. Greer, "Dose-to-water conversion for the backscatter-shielded EPID: A frame-based method to correct for EPID energy response to MLC transmitted radiation," Medical Physics **41**, 081716 (2014).
[32] B. Liu, J. Adamson, A. Rodrigues, F. Zhou, F.-f. Yin, Q. Wu, "A novel technique for VMAT QA with EPID in cine mode on a Varian TrueBeam linac," Physics in Medicine and Biology **58**, 6683 (2013).
[33] T. Fuangrod, H.C. Woodruff, E. van Uytven, B.M.C. McCurdy, Z. Kuncic, D.J. O'Connor, P.B. Greer, "A system for EPID-based real-time treatment delivery verification during dynamic IMRT treatment," Medical Physics **40**, - (2013).
[34] W. Ansbacher, C.L. Swift, P.B. Greer, "An evaluation of cine-mode 3D portal image dosimetry for volumetric modulated arc therapy," Journal of Physics: Conference Series **250**, 108-111 (2010).

[35] W. Ansbacher, "Three-dimensional portal image-based dose reconstruction in a virtual phantom for rapid evaluation of IMRT plans," Medical Physics **33**, 3369-3382 (2006).
[36] H.C. Woodruff, T. Fuangrod, P. Rowshanfarzad, B.M.C. McCurdy, P.B. Greer, "Gantry-angle resolved VMAT pretreatment verification using EPID image prediction," Medical Physics **40**, - (2013).
[37] A. Mans, D. Schuring, M.P. Arends, C.A.Vugts, J.W. Wolthaus, H.T. Lotz, M. Admiraal, R.J. Louwe, M.C. Öllers, J.B. van de Kamer, "The NCS code of practice for the quality assurance and control for volumetric modulated arc therapy", Physics of Medicine and Biology **61**, 7221 (2016).
[38] H.C. Woodruff, P.B. Greer, "3D Dose reconstruction: Banding artefacts in cine mode EPID images during VMAT delivery," Journal of Physics: Conference Series **444**, 012042 (2013).
[39] P. Vial, L. Oliver, P.B. Greer, C. Baldock, "An experimental investigation into the radiation field offset of a dynamic multileaf collimator," Physics in Medicine and Biology **51**, 5517-5538 (2006).
[40] M. Partridge, P.M. Evans, A. Mosleh-Shirazi, D. Convery, "Independent verification using portal imaging of intensity-modulated beam delivery by the dynamic MLC technique," Medical Physics **25**, 1872-1879 (1998).
[41] M.S. Bhagwat, Z. Han, S.K. Ng, P. Zygmanski, "An oscillating sweeping gap test for VMAT quality assurance," Physics in Medicine and Biology **55**, 5029 (2010).
[42] P.B. Greer, "Off-axis dose response characteristics of an amorphous silicon electronic portal imaging device," Medical Physics **34**, 3815-3824 (2007).
[43] E.E. Klein, J. Hanley, J. Bayouth, F.-F. Yin, W. Simon, S. Dresser, C. Serago, F. Aguirre, L. Ma, B. Arjomandy, "Task Group 142 report: Quality assurance of medical accelerators," Medical Physics **36**, 4197-4212 (2009).
[44] M. Oliver, I. Gagne, K. Bush, S. Zavgorodni, W. Ansbacher, W. Beckham, "Clinical significance of multi-leaf collimator positional errors for volumetric modulated arc therapy," Radiotherapy and oncology : journal of the European Society for Therapeutic Radiology and Oncology **97**, 554-560 (2010).
[45] G.J. Kutcher, L. Coia, M. Gillin, W.F. Hanson, S. Leibel, R.J. Morton, J.R. Palta, J.A. Purdy, L.E. Reinstein, G.K. Svensson, "Comprehensive QA for radiation oncology: report of AAPM radiation therapy committee task group 40," Medical physics **21**, 581-618 (1994).
[46] M.S. Huq, B.A. Fraass, P.B. Dunscombe, J.P. Gibbons, G.S. Ibbott, A.J. Mundt, S. Mutic, J.R. Palta, F. Rath, B.R. Thomadsen, "The report of Task Group 100 of the AAPM: Application of risk analysis methods to radiation therapy quality management," Medical Physics **43**, 4209-4262 (2016).
[47] J. Adamson, Q. Wu, "Independent verification of gantry angle for pre-treatment VMAT QA using EPID," Physics in Medicine and Biology **57**, 6587 (2012).

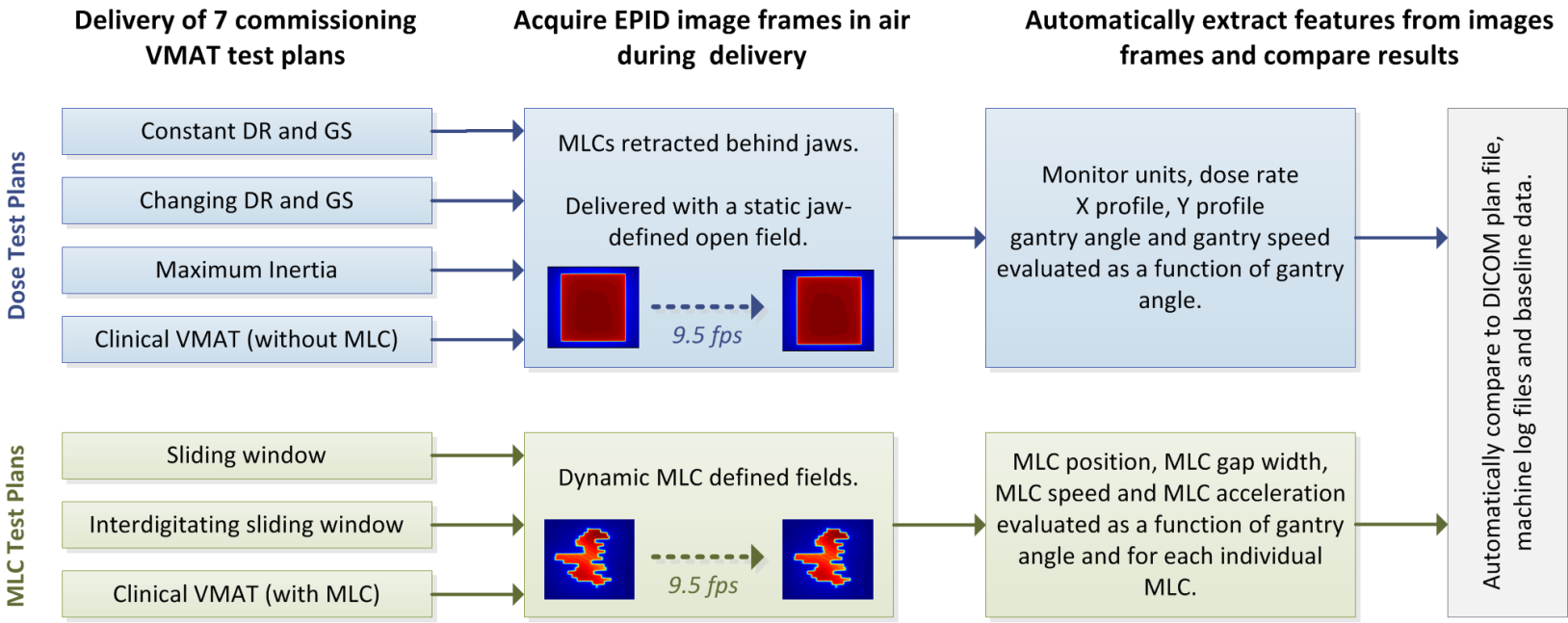
Delivery of 7 commissioning VMAT test plans
Acquire EPID image frames in air during delivery
Automatically extract features from images frames and compare results
Dose Test Plans
Constant DR and GS
Changing DR and GS
Maximum Inertia
Clinical VMAT (without MLC)
MLCs retracted behind jaws.
Delivered with a static jaw-defined open field.
9.5 fps
Monitor units, dose rate
X profile, Y profile
gantry angle and gantry speed
evaluated as a function of gantry angle.
MLC Test Plans
Sliding window
Interdigitating sliding window
Clinical VMAT (with MLC)
Dynamic MLC defined fields.
9.5 fps
MLC position, MLC gap width, MLC speed and MLC acceleration evaluated as a function of gantry angle and for each individual MLC.
Automatically compare to DICOM plan file, machine log files and baseline data.

(a) MLC Test 1:
Sliding Window

Start of Seg:

Bank A +7 cm
Bank B -5 cm

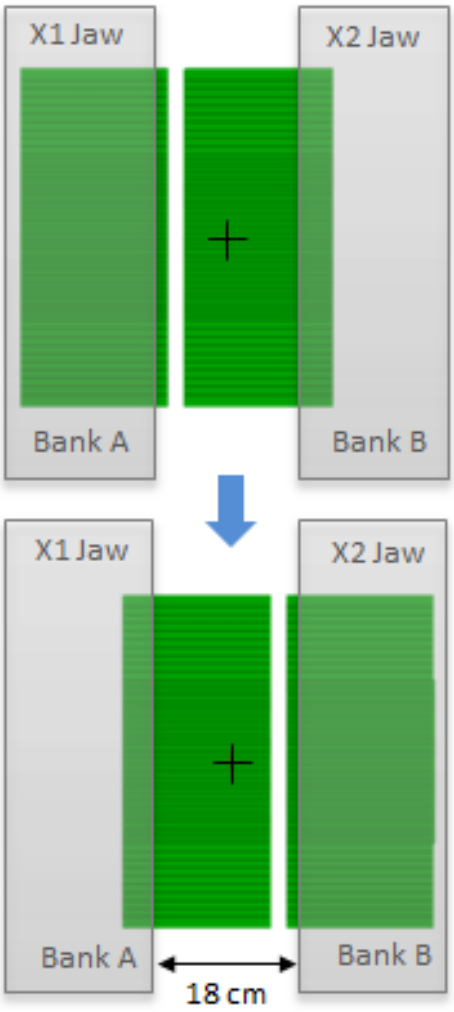

End of Seg:

Bank A -5 cm
Bank B +7 cm

(b) MLC Test 2:
Interdigitating Sliding Window

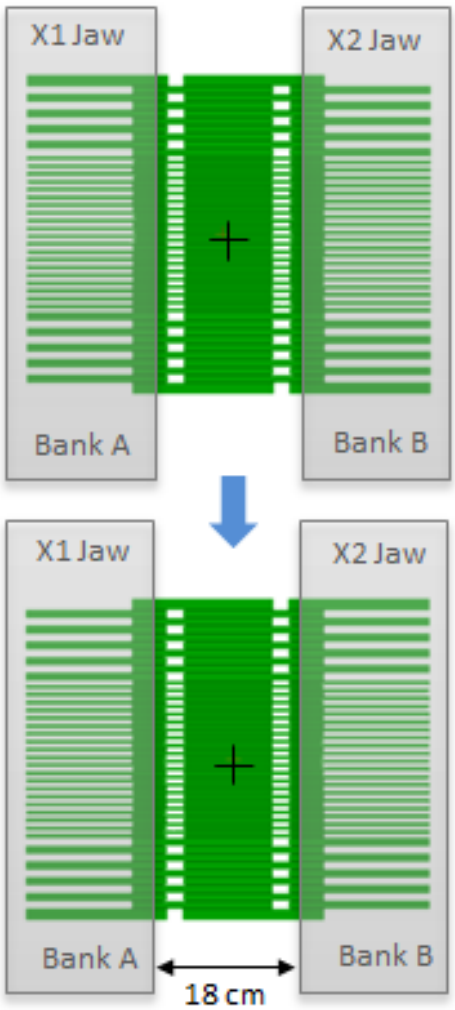

Start of Seg:

Bank A (odd) +7 cm
Bank B (odd) -5 cm

Bank A (even) -5 cm
Bank B (even) +7 cm

End of Seg:

Bank A (odd) -5 cm
Bank B (odd) +7 cm

Bank A (even) +7 cm
Bank B (even) -5 cm

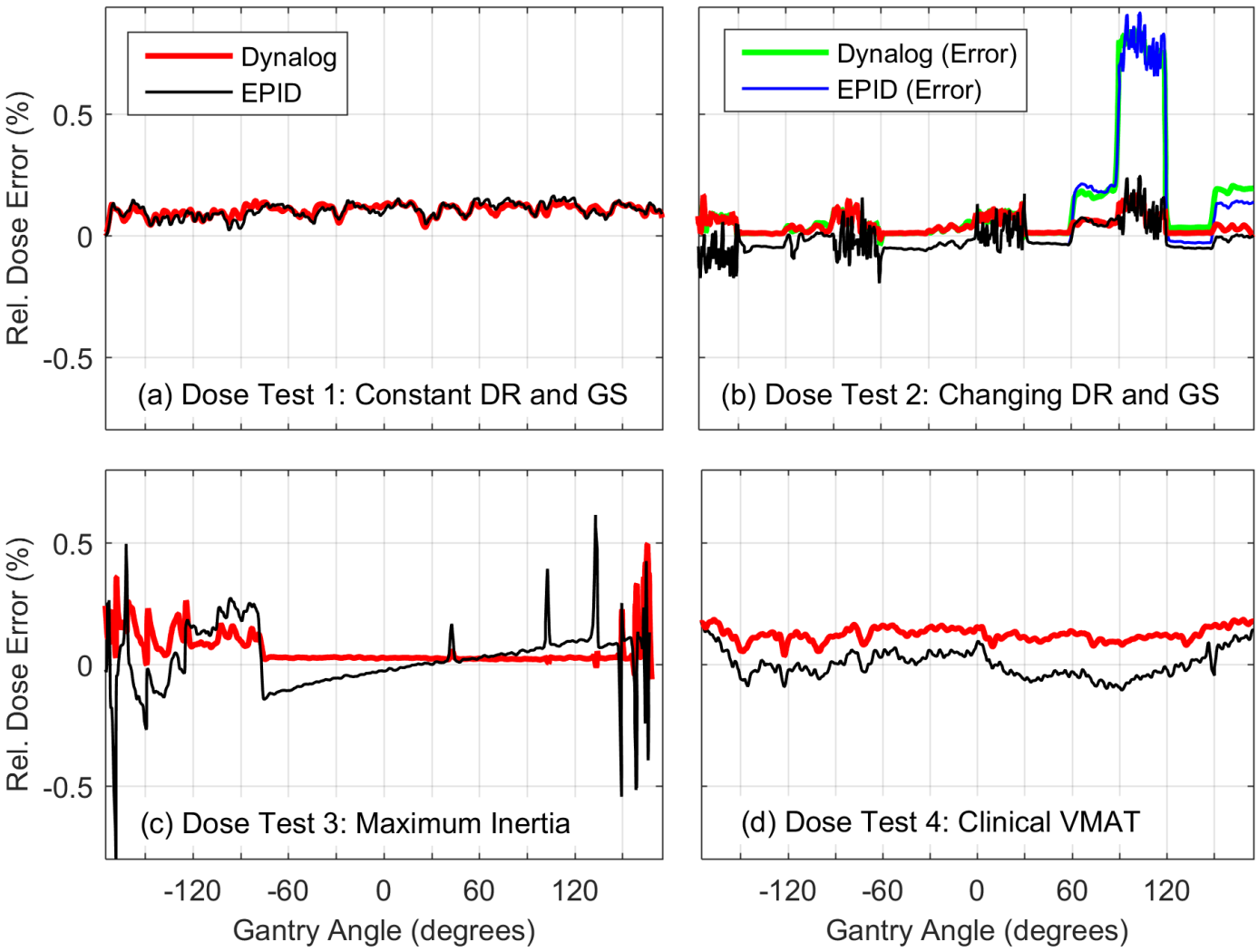
Dynalog
EPID
Rel. Dose Error (%)
0.5
0
-0.5
(a) Dose Test 1: Constant DR and GS
Dynalog (Error)
EPID (Error)
(b) Dose Test 2: Changing DR and GS
(c) Dose Test 3: Maximum Inertia
(d) Dose Test 4: Clinical VMAT
-120
-60
0
60
120
Gantry Angle (degrees)

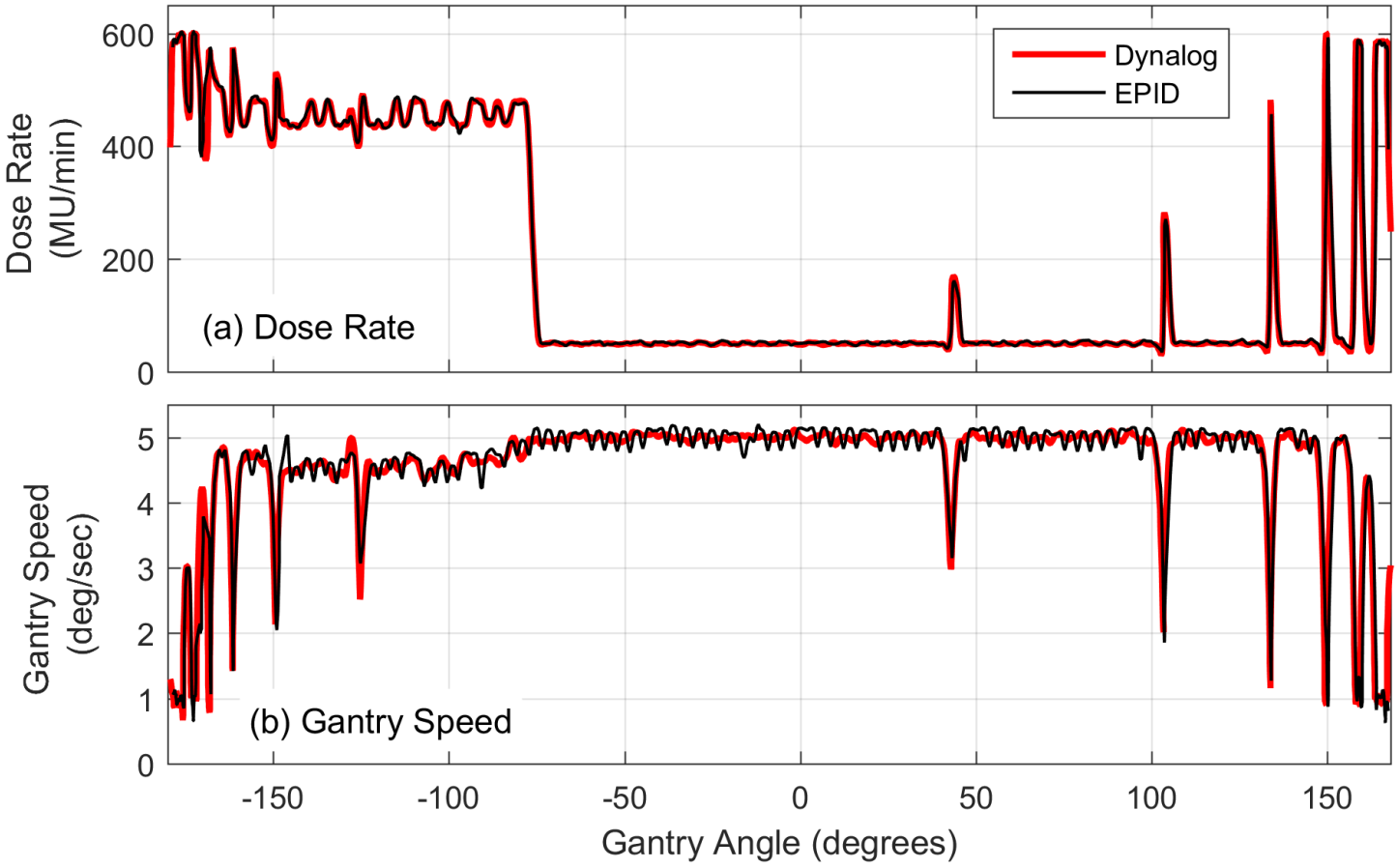
Dose Rate
(MU/min)
600
400
200
0
Dynalog
EPID
(a) Dose Rate
Gantry Speed
(deg/sec)
5
4
3
2
1
0
(b) Gantry Speed
-150
-100
-50
0
50
100
150
Gantry Angle (degrees)

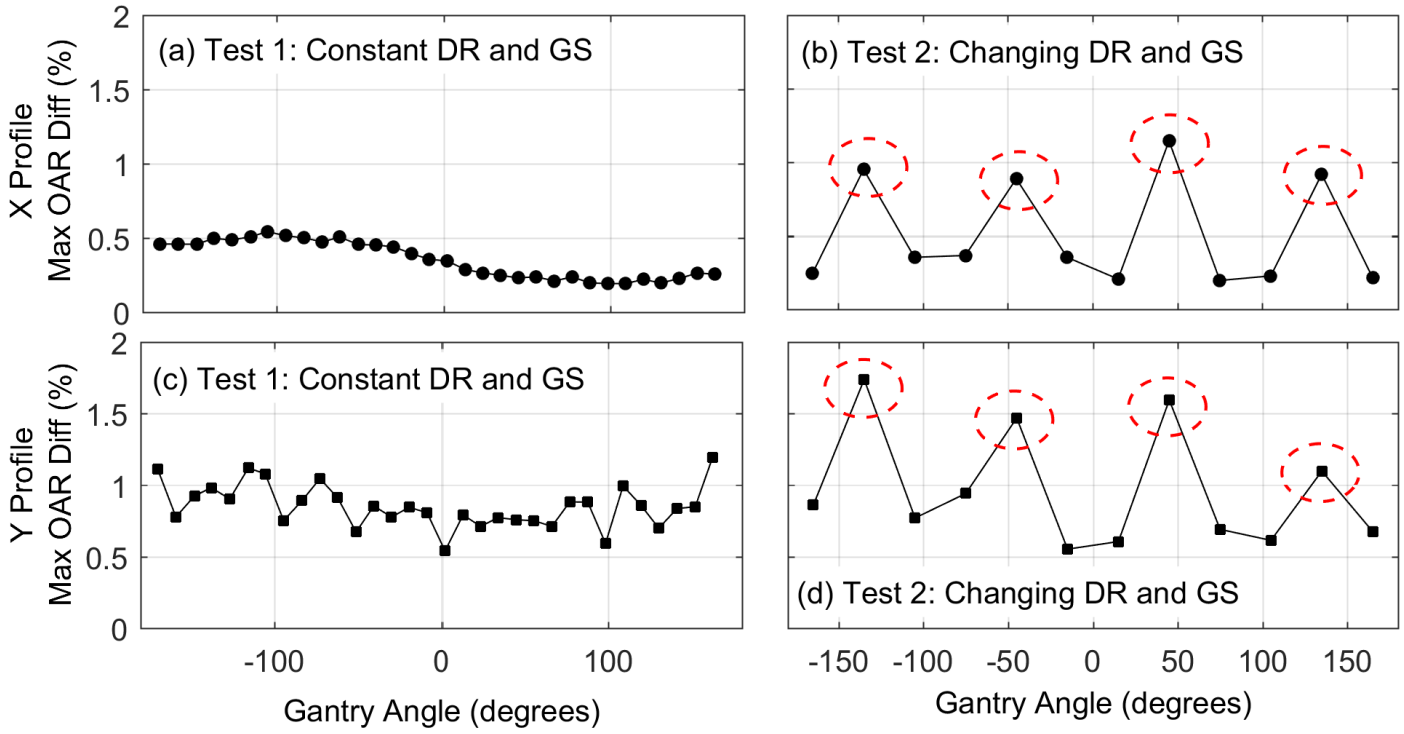
(a) Test 1: Constant DR and GS
(b) Test 2: Changing DR and GS
(c) Test 1: Constant DR and GS
(d) Test 2: Changing DR and GS
X Profile
Max OAR Diff (%)
Y Profile
Max OAR Diff (%)
0
0.5
1
1.5
2
-100
0
100
-150
-100
-50
0
50
100
150
Gantry Angle (degrees)
Gantry Angle (degrees)

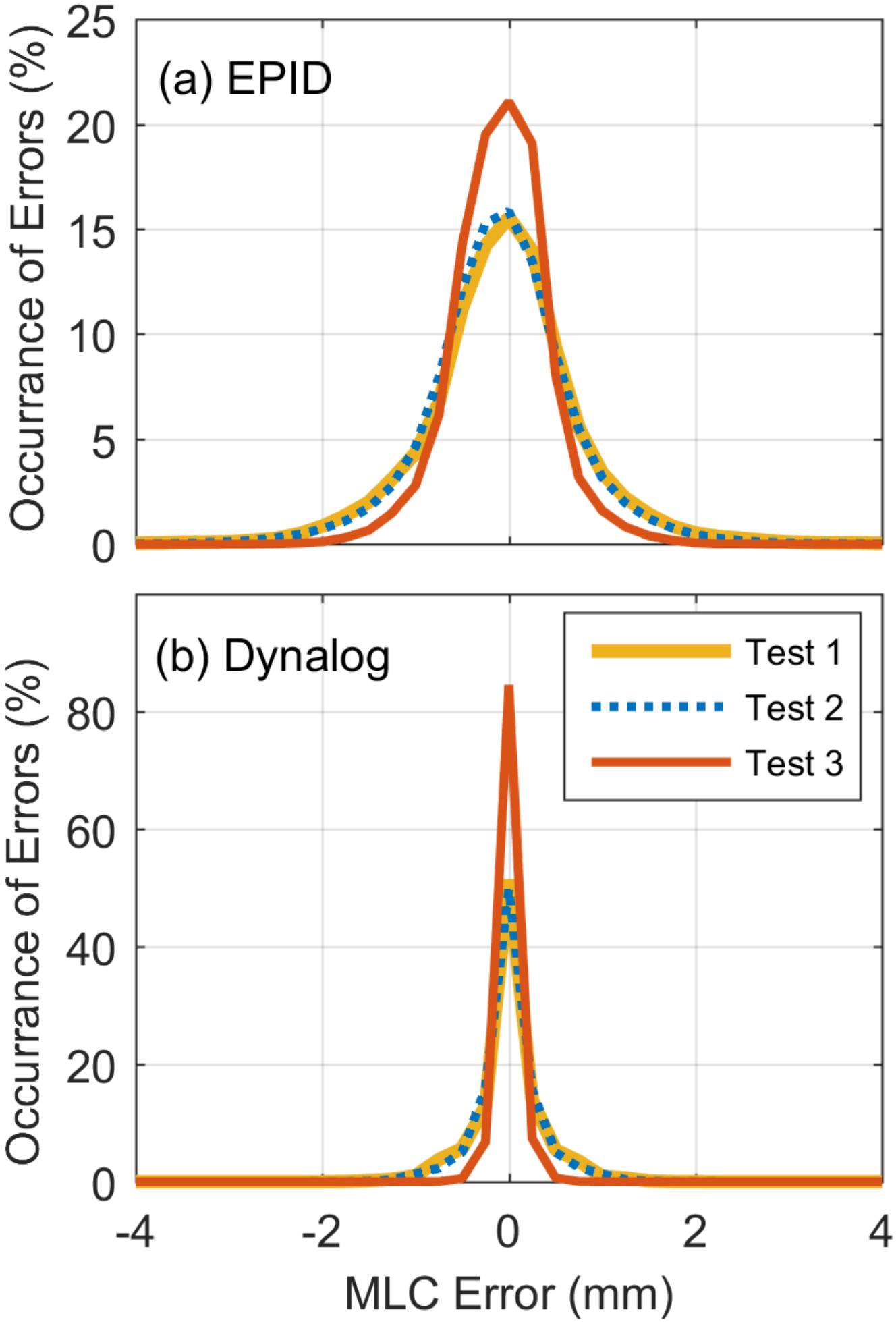
(a) EPID
Occurrance of Errors (%)
25
20
15
10
5
0
(b) Dynalog
Occurrance of Errors (%)
80
60
40
20
0
Test 1
Test 2
Test 3
-4
-2
0
2
4
MLC Error (mm)

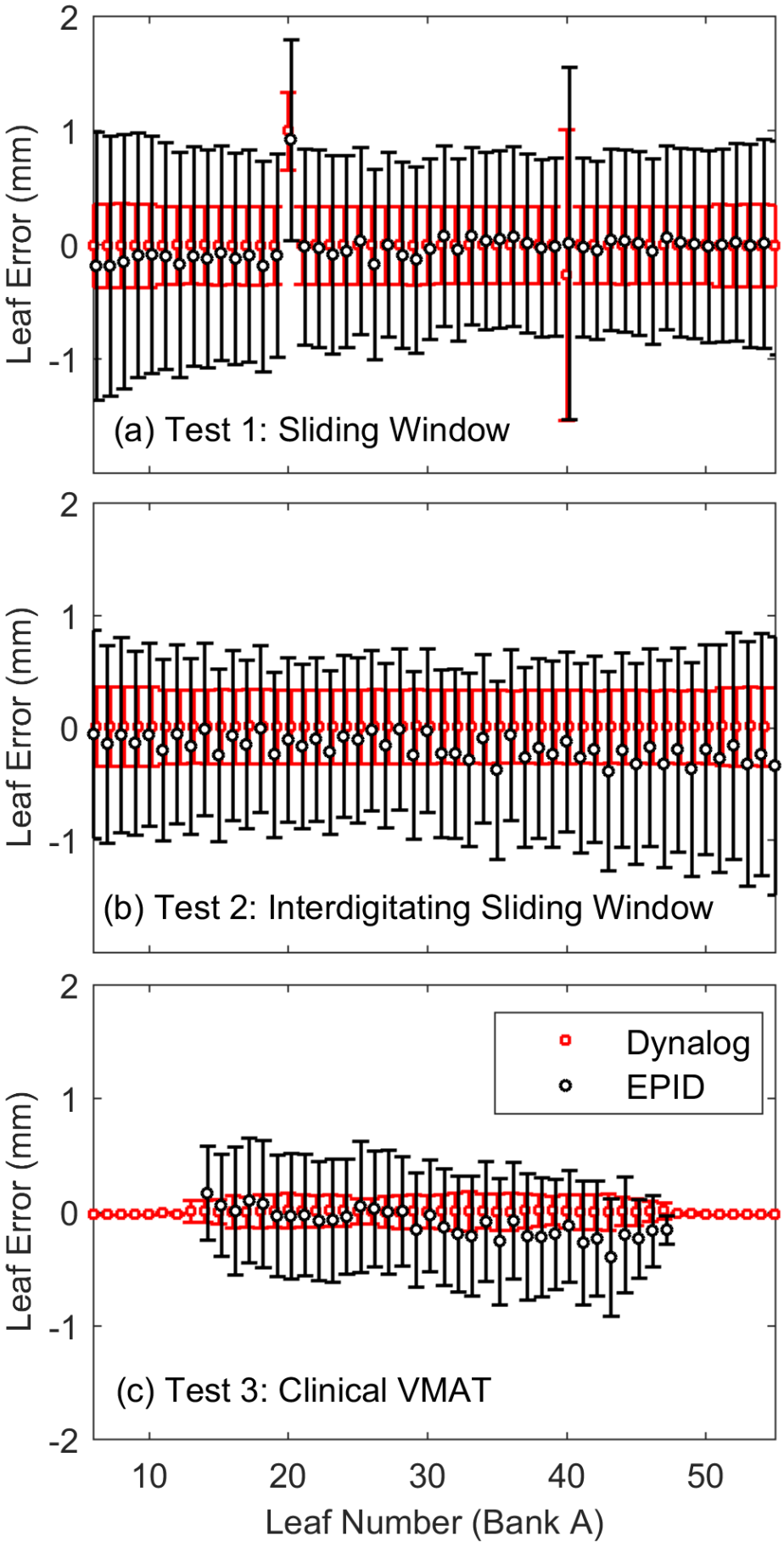
Leaf Error (mm)
2
1
0
-1
(a) Test 1: Sliding Window
Leaf Error (mm)
2
1
0
-1
(b) Test 2: Interdigitating Sliding Window
Leaf Error (mm)
2
1
0
-1
-2
Dynalog
EPID
(c) Test 3: Clinical VMAT
10
20
30
40
50
Leaf Number (Bank A)

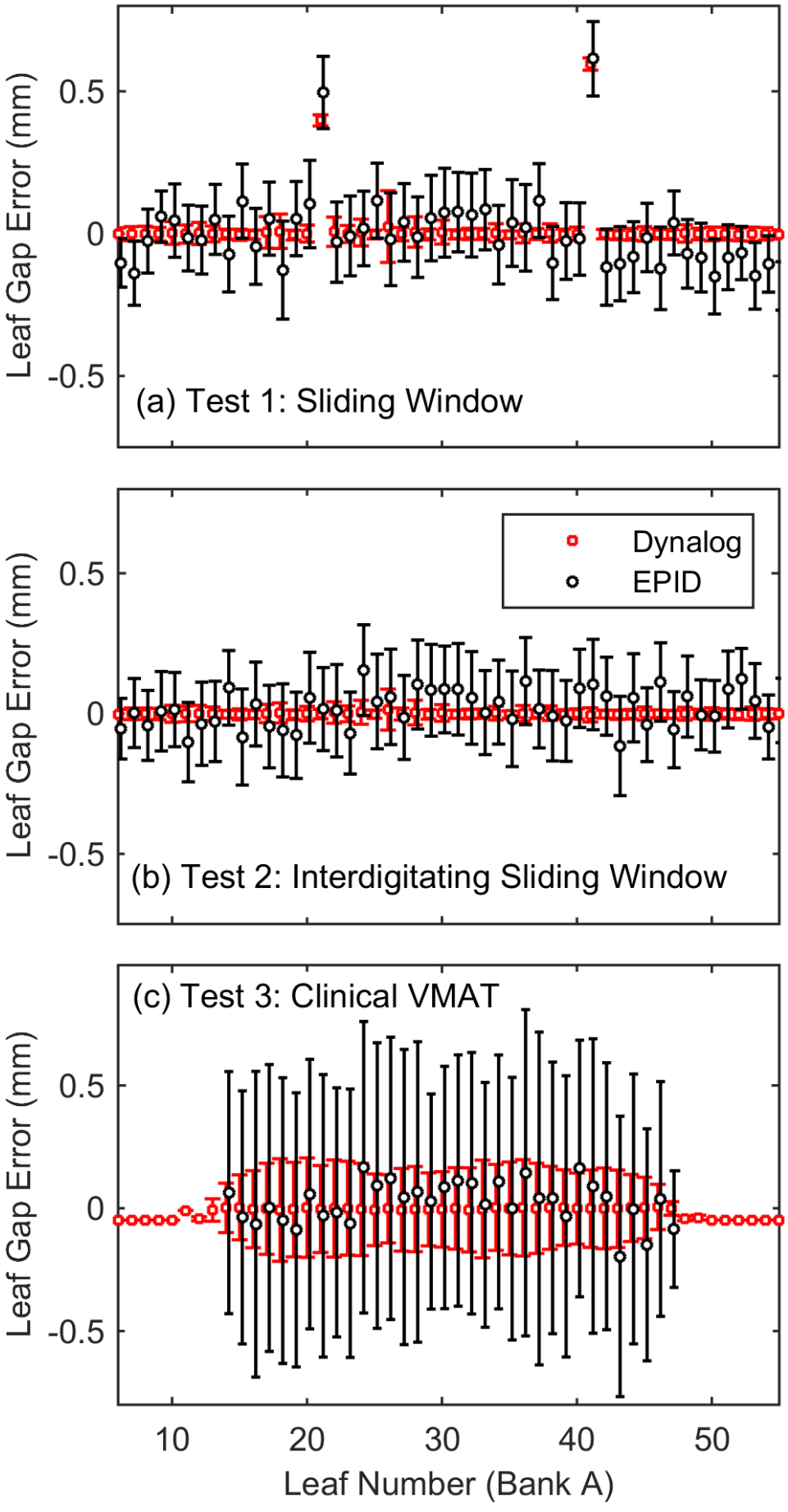
Leaf Gap Error (mm)
0.5
0
-0.5
(a) Test 1: Sliding Window
Dynalog
EPID
(b) Test 2: Interdigitating Sliding Window
(c) Test 3: Clinical VMAT
10
20
30
40
50
Leaf Number (Bank A)

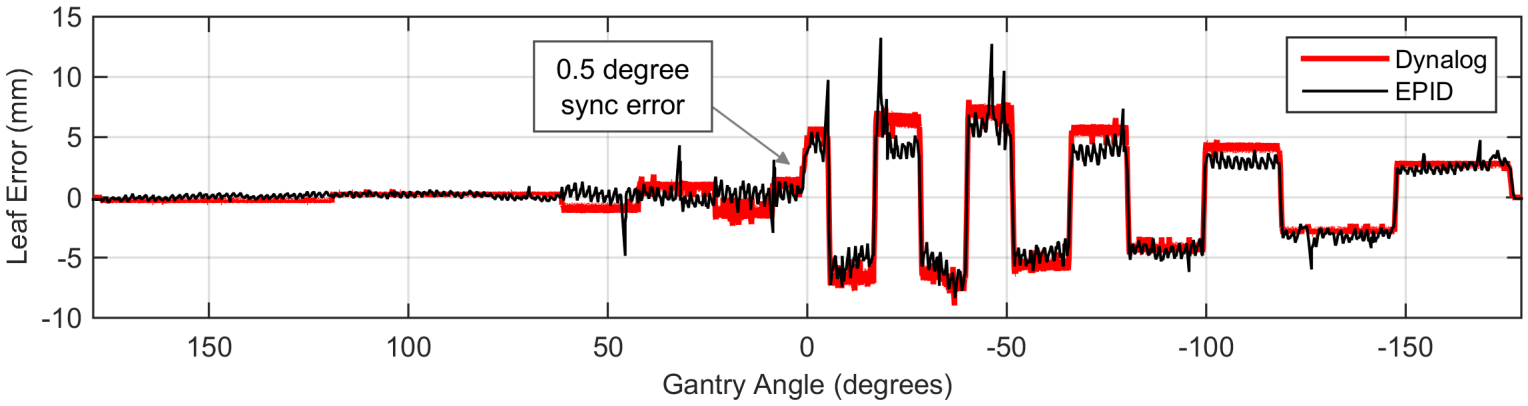
15
10
5
0
-5
-10
Leaf Error (mm)
150
100
50
0
-50
-100
-150
Gantry Angle (degrees)
0.5 degree
sync error
Dynalog
EPID

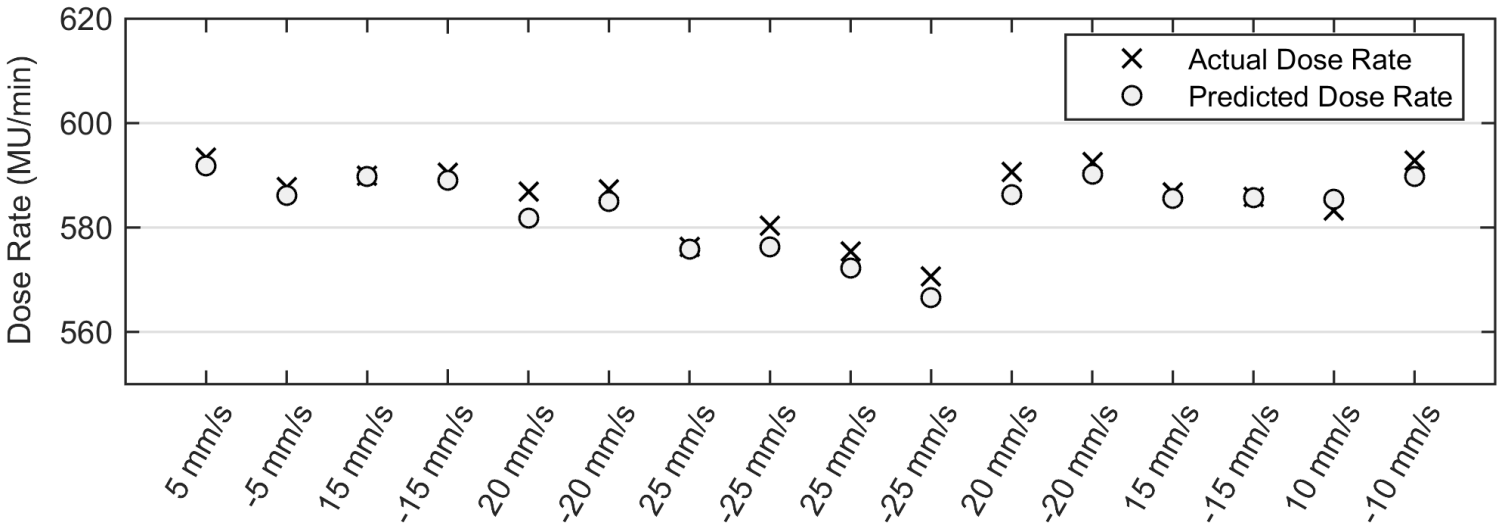
620
600
580
560
Dose Rate (MU/min)
Actual Dose Rate
Predicted Dose Rate
5 mm/s
-5 mm/s
15 mm/s
-15 mm/s
20 mm/s
-20 mm/s
25 mm/s
-25 mm/s
25 mm/s
-25 mm/s
20 mm/s
-20 mm/s
15 mm/s
-15 mm/s
10 mm/s
-10 mm/s

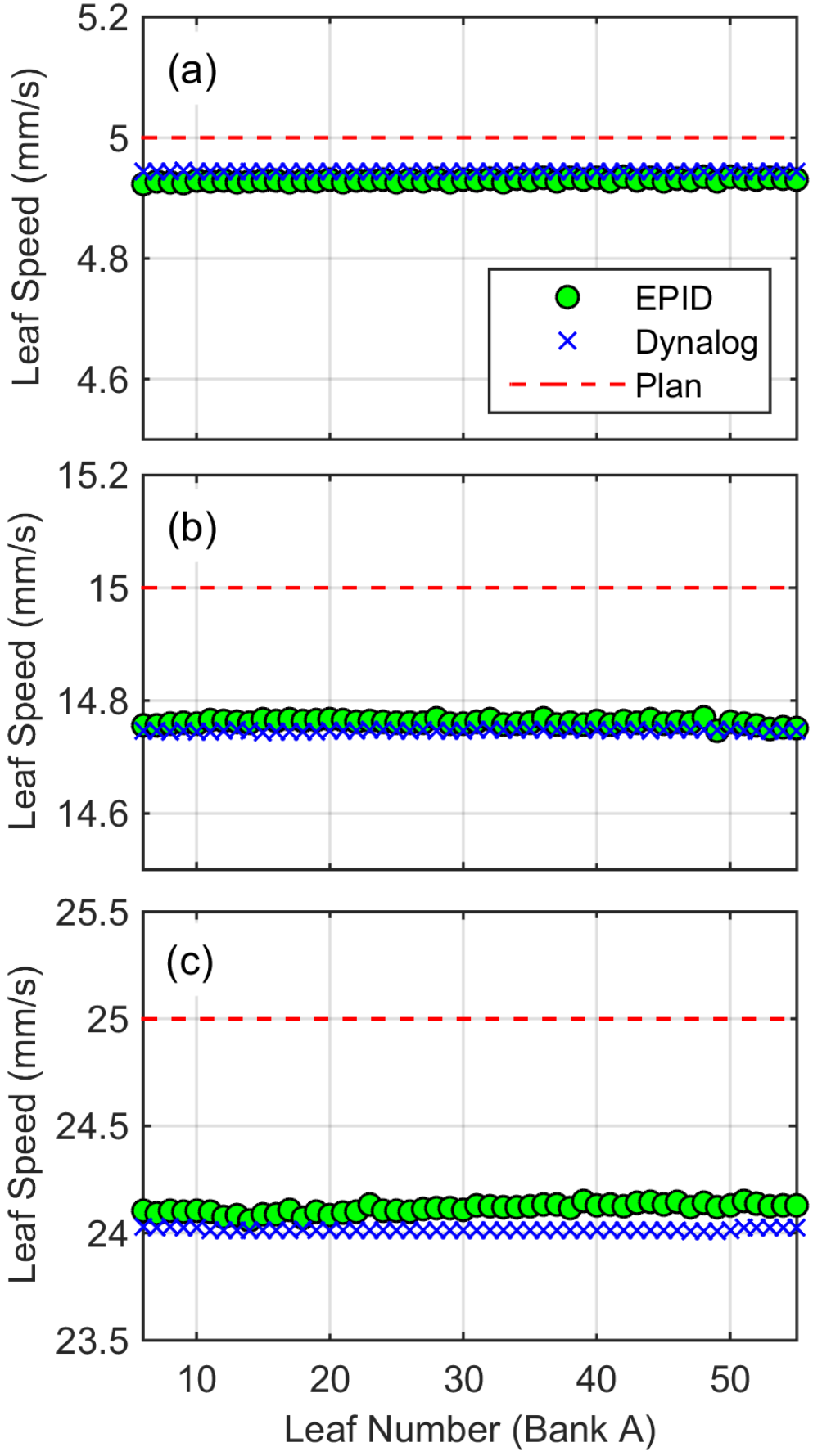
(a)
(b)
(c)
Leaf Speed (mm/s)
Leaf Speed (mm/s)
Leaf Speed (mm/s)
5.2
5
4.8
4.6
15.2
15
14.8
14.6
25.5
25
24.5
24
23.5
EPID
Dynalog
Plan
10
20
30
40
50
Leaf Number (Bank A)